Mid-Course Assessment

Hierarchically Modelling Stars Using Deep Learning and Asteroseismology

By

Alexander J. Lyttle

Student ID 1532473
Supervisor Dr Guy R. Davies
Co-Supervisor Dr Andrea Miglio

Solar and Stellar Physics Group
School of Physics and Astronomy
College of Engineering and Physical Sciences
University of Birmingham

September 14, 2020

ABSTRACT

Your abstract goes here

ACKNOWLEDGMENTS

I acknowledge the people who helped me.

Contents

List of Figures

List of Tables

Chapter 1

Introduction

1.1 Hierarchical Bayesian Models

Consider a model for a single object comprising a set of independent parameters, $\boldsymbol{\theta} = \{\theta_i\}_{i=1}^{N_\theta}$ which makes a set of predictions, $\boldsymbol{\mu}_y = \{\mu_{y,j}\}_{j=1}^{N_y}$ where $\boldsymbol{\mu}_y = \boldsymbol{f}(\boldsymbol{\theta})$. Using Bayes' theorem, we may write the *posterior* probability density function (PDF) of the model given a set of observations $\boldsymbol{y}$ as,

$$p(\boldsymbol{\theta}|\boldsymbol{y}) = \frac{p(\boldsymbol{y}|\boldsymbol{\theta})\, p(\boldsymbol{\theta})}{p(\boldsymbol{y})}, \tag{1.1}$$

where $p(\boldsymbol{y}|\boldsymbol{\theta})$ is the *likelihood* of the data given the model, $p(\boldsymbol{\theta})$ is the *a priori* PDF of the model parameters, and $p(\boldsymbol{y})$ is the *evidence* of the data.

Assuming our observations of $\boldsymbol{y}$ are uncorrelated and subjected to random, Gaussian noise with a known standard deviation, $\boldsymbol{\sigma}_y$, we may write the likelihood function as a normal distribution,

$$p(\boldsymbol{y}|\boldsymbol{\theta}) = \prod_{j=1}^{N_y} \frac{1}{\sigma_{y,j}\sqrt{2\pi}} \exp\left[-\frac{(y_j - \mu_{y,j})^2}{2\sigma_{y,j}^2}\right], \tag{1.2}$$

$$\equiv \prod_{j=1}^{N_y} \mathcal{N}(y_j|\mu_{y,j}, \sigma_{y,j}). \tag{1.3}$$

The prior PDF of the model, assuming the parameters are independent, is $p(\boldsymbol{\theta}) = \prod_i p(\theta_i)$. Encoding our prior understanding of the model this way is useful for improving our inference. For example, we have independent evidence that the age of the universe is $\sim 14\,\mathrm{Gyr}$ [CITE]. Hence, we may choose to give the age parameter for a stellar model a uniform prior PDF from 0 to 14 Gyr such that our posterior PDF is not influenced by unphysical ages.

The evidence is the PDF of the observational data. We write this as the normalisation of the numerator of Equation 1.1,

$$p(\boldsymbol{y}) = \int_{-\infty}^{+\infty} p(\boldsymbol{y}|\boldsymbol{\theta})\, p(\boldsymbol{\theta})\, \mathrm{d}\boldsymbol{\theta}. \tag{1.4}$$

There are many ways to determine the posterior PDF, either analytically or numerically using e.g. Markov chain Monte Carlo (MCMC) through algorithms such as Metropolis-Hastings and Hamiltonian Monte-Carlo (HMC) [CITE]. Once we have the posterior, we can determine the marginalised posterior distribution of an individual parameter by integrating over all other parameters. For example, the marginalised posterior for θ_1 is,

$$p(\theta_1|\boldsymbol{y}) = \int_{-\infty}^{+\infty} p(\boldsymbol{\theta}|\boldsymbol{y})\, \mathrm{d}\theta_2 \ldots \mathrm{d}\theta_{N_\theta}. \tag{1.5}$$

Therefore, we end up with a distribution which describes the probability of θ_1 given $\boldsymbol{y}$ which takes into account the distribution (or uncertainty) of all other parameters in the model.

The model described above can be applied to a single object such as a star. Let us now consider modelling a population of N_{obj} similar objects. We could combine the posteriors for each object to get a posterior for the population of objects,

$$p(\boldsymbol{\Theta}|\boldsymbol{Y}) = \prod_{k=1}^{N_{\mathrm{obj}}} p(\boldsymbol{\theta}_k|\boldsymbol{y}_k), \tag{1.6}$$

where $\boldsymbol{\Theta} = \{\boldsymbol{\theta}_k\}_{k=1}^{N_{\mathrm{obj}}}$ and $\boldsymbol{Y} = \{\boldsymbol{y}_k\}_{k=1}^{N_{\mathrm{obj}}}$ are the matrices of model parameters and observations. We refer to this as a *no-pooled* model because no information is shared between the objects. However, what if we have a model which describes the distribution of a particular $\boldsymbol{\theta}_i$ in the population? For

example, if all the objects are stars in an open cluster which formed at roughly the same time, such as Messier 67 [CITE], we might want to encode such information into the model. One method would be to independently model the stars in the cluster and then find their population mean and standard deviation in age. It has been shown that this method typically over-predicts the standard deviation because it propagates the object-level uncertainties [CITE]. Alternatively, we can incorporate the assumption that stars in a cluster formed at the same time using one of two ways. The first is to *partially-pool* and the second is to *max-pool* the stellar ages respectively. The former assumes the object-level parameters are drawn from some common distribution, and the latter is the special case where all object-level parameters share the same value in the population.

We refer to models which pool parameters in this way as hierarachical models [CITE]. We describe the distribution of $\boldsymbol{\Theta}$ in the population by a set of *hyper-parameters*, $\boldsymbol{\phi} = \{\phi_l\}_{l=1}^{N_\phi}$. Bayes' equation now becomes,

$$p(\boldsymbol{\phi}, \boldsymbol{\Theta}|\boldsymbol{Y}) = \frac{p(\boldsymbol{Y}|\boldsymbol{\Theta})\, p(\boldsymbol{\Theta}|\boldsymbol{\phi})\, p(\boldsymbol{\phi})}{p(\boldsymbol{Y})} \tag{1.7}$$

where the probability of $\boldsymbol{\Theta}$ given $\boldsymbol{\phi}$ is,

$$p(\boldsymbol{\Theta}|\boldsymbol{\phi}) = \prod_{k=1}^{N_{\text{obj}}} d(\boldsymbol{\theta}_k|\boldsymbol{\phi}), \tag{1.8}$$

and $d(\boldsymbol{\theta}_k|\boldsymbol{\phi})$ is some chosen distribution from which the parameters for a given object are drawn from the population.

Let us consider a simple model which predicts the luminosities, $\boldsymbol{L}$ from the ages, $\boldsymbol{\tau}$ of $N_{\text{obj}} = 1000$ stars in a cluster formed at roughly the same time. Modelling the population independently, we get the posterior,

$$p(\boldsymbol{\tau}|\boldsymbol{L}) \propto \prod_{k=1}^{1000} p(L_k|\tau_k)\, p(\tau_k). \tag{1.9}$$

Now, let us consider a partially-pooled model where the stellar ages are drawn from a normal distribution centred on a mean, μ_τ and standard deviation, σ_τ. The posterior now becomes,

$$p(\mu_\tau, \sigma_\tau, \boldsymbol{\tau}|\boldsymbol{L}) \propto p(\boldsymbol{L}|\boldsymbol{\tau})\, p(\boldsymbol{\tau}|\mu_\tau, \sigma_\tau)\, p(\mu_\tau, \sigma_\tau), \tag{1.10}$$

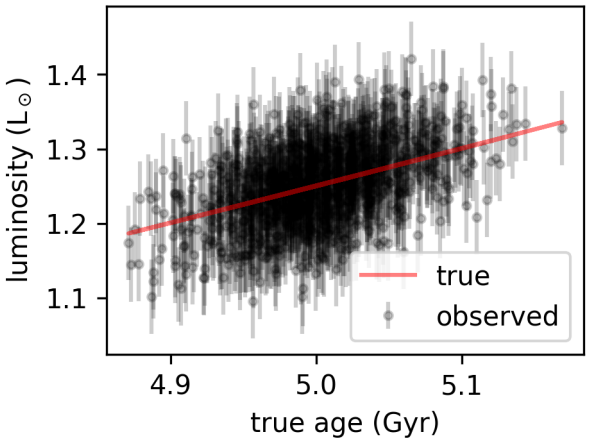

Figure 1.1: Luminosity against true ages of a fake stellar cluster. The true luminosities lie on the red line and the observed luminosities (black) have been artificially scattered by $0.05\,L_\odot$.

where,

$$p(\boldsymbol{\tau}|\mu_\tau, \sigma_\tau) = \prod_{k=1}^{1000} \mathcal{N}(\tau_k|\mu_\tau, \sigma_\tau). \tag{1.11}$$

There is no known analytical or empirical relation between the age of a star and its luminosity, but for the purposes of this example let us say that we know $L \propto \tau^2$. I generated 1000 stellar ages from a normal distribution with a mean of 5 Gyr and a standard deviation of 0.05 Gyr, and computed their luminosities using this relation. Then, I added Gaussian noise to the luminosities with a standard deviation of $0.05\,L_\odot$ and proceeded to model the stellar ages using Equations 1.9 and 1.10 and the Bayesian package `pymc3` [CITE]. The observed and true luminosities are plot against the true ages in Figure 1.1 to show

If we wished to determine spread of stellar ages in the cluster using the no-pooled model, we might naïvely calculate a standard deviation from the resulting stellar ages. However, this overestimates the true standard deviation, getting 0.109 Gyr rather than 0.05 Gyr, because it includes the uncertainty in the individual ages. When we model the population mean and spread in the hierarchical model we get $\mu_\tau = 5.002 \pm 0.003$ Gyr and $\sigma_\tau = 0.042 \pm 0.007$ Gyr which are within $< 2\sigma$ of the truths. Therefore, the hierarachical model is a better way of determining population-

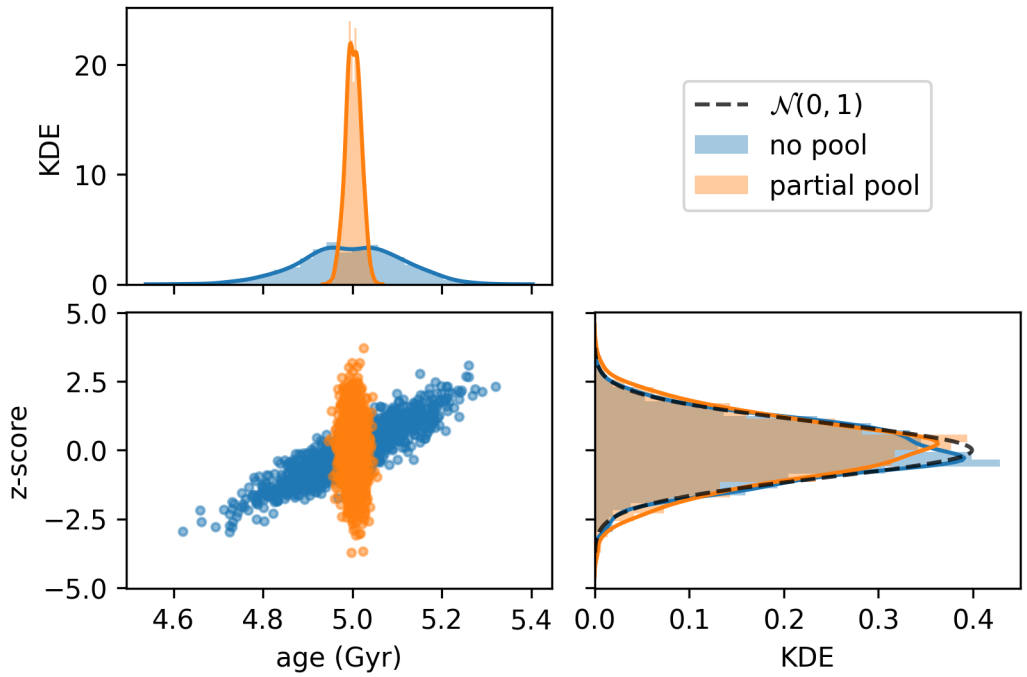

Figure 1.2: The z-score, $(\bar{\tau} - \tau_{\text{true}})/s_\tau$, where $\bar{\tau}$ and s_τ are the respective sample mean and standard deviation of the posterior ages from each of the no- and partially-pooled models.

level statistics than the traditional no-pooled model.

Both models can accurately determine ages, but the hierarchical model returns more precise ages, assuming our prior assumptions are true. Figure 1.2 shows that the z-score for ages from both models match a normal distribution with a mean of 0 and standard deviation of 1, indicating the individual stellar ages and uncertainties are accurate. However, the partially pooled model produces more than doubly precise ages, as shown in Figure 1.3, because the model takes into account the population mean and spread as hyper-parameters. The reduced scatter on stellar ages is also reflected in the top-left plot of Figure 1.2.

If we wish to improve the precision of fundamental stellar parameters, using hierarchical models to encode our prior knowledge is essential. However, modelling stars is not as simple, nor analytical as in the example above. Before we can statistically model a population of stars, we must

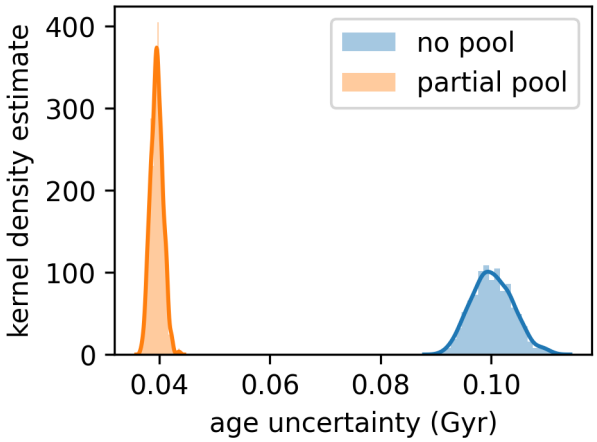

Figure 1.3: Standard deviations, s_τ of the age posteriors from both the no- and partially-pooled models.

have a way of generating stellar observables from fundamental parameters such as age and mass. In the next section, I give an overview of how we numerically model stellar observables and why traditional methods pose new problems when adapting the above model.

1.2 Modelling a Star

How do we model stellar observables? A bit of history of the topic including Eddington (1926). Then Chandrasekhar 1939 and Schwartzschild 1958.

Introduction of stellar computational codes in the 1960s e.g. Iben and Ehrman 1962 and Kippenhahn et al. 1967 to solve the complicated differential equations

Today, many codes exist from one-dimensional [CITE] to three-dimensional and their outputs are often compared [CITE aarhus red giants challenge and Magic papers].

Why did we chose MESA?

What are the basic need-to-knows of stellar evolution in order to understand this work?

Basic scalings of observables with fundamentals, e.g. what is luminosity, effective temperature.

What are the evolutionary phases, a stellar track may be useful here?

What is X Y and Z and w

What is the mixing-length theory of convection? A diagram of the sun may be helpful.

What is element diffusion and why is it better to include it?

Finally, what is asteroseismology and why is it useful in stellar evolution?

1.3 Astroseismology

For over a century, we have been able to map stars based on their photometric magnitude and spectroscopic colour using Hertzsprung-Russell (HR) diagrams. Coupling such observational data with measurements of interstellar distances using parallax, we were able to determine stellar luminosities. The unique structure of early HR diagrams eluded to the idea that stars evolve over time. With the addition of nuclear physics, theories of stellar evolution could be put to the test. However, while we could only observe stellar surface properties, many modelling mysteries would be left unsolved.

Until the last few decades, our understanding of stellar structure has been all but skin deep. In the 1960s, observations of 5-minute brightness fluctuations in the solar photosphere lead to the study of stochastically driven acoustic waves trapped beneath the surface of the Sun (Ulrich, 1970; Ando and Osaki, 1975). Later named helioseismology (Deubner and Gough, 1984), the

study of oscillation modes allowed for further insights into the solar interior, such as rotation (Deubner, Ulrich, and Rhodes, 1979) and solar neutrino production (Bahcall and Ulrich, 1988). In tandem with this research was the emergence of asteroseismology – the study of stars through their oscillation frequencies (Christensen-Dalsgaard, 1984).

Give examples of the sorts of things asteroseismology can help us uncover, from ages (Ulrich, 1986; Soderblom, 2010; Silva Aguirre, Davies, et al., 2015, see, e.g.) to masses and radii from scaling relations () and fitting stellar models().

1.3.1 Solar-like oscillators

Solar-like oscillators are stars which typical exhibit two kinds of standing waves: acoustic oscillation modes (or p modes) excited stochastically by convection in their outer layers and restored by pressure gradients, and internal gravity waves (or g modes) which are controlled by buoyancy. This work focuses on main sequence stars for which p modes are only present in their spectra. Hence, in this section I will summarise the theory behind acoustic waves present in main sequence stars.

The theory which predicts the locations of the asteroseismic oscillation modes has its roots in the spherical harmonic oscillator. The eigenfrequencies, ν_{nlm} are categorised into modes of radial order, n, angular degree, l and in the case of rotating bodies, azimuthal order, m. To simplify this discussion, I will assume the case where the star is non-rotating.

To first order in $\Delta\nu$, I may express the eigenfrequency as follows [CITE],

$$\nu_{nl} \simeq \Delta\nu \left(n + \frac{l}{2} + \epsilon \right) \tag{1.12}$$

where,

$$\Delta\nu = \left(2 \int_0^R \frac{\mathrm{d}r}{c(r)} \right)^{-1} \tag{1.13}$$

is proportional to the inverse of the sound travel time over the stellar diameter, $2R$ where the speed

of sound c is a function of stellar radii. The large frequency separation, $\Delta\nu$ is approximately the frequency difference between consecutive modes of the same l. From Equation 1.13, it has been shown by substitution of the speed of sound in a gas, that the average large frequency separation, $\langle\Delta\nu\rangle$ scales with the average stellar density, $\langle\rho\rangle$ [CITE Ulrich 1989],

$$\langle\Delta\nu_{nl}\rangle \propto \langle\rho\rangle^{1/2}. \tag{1.14}$$

The diagram in Figure **??** shows the path of the asteroseismic wave fronts through a cross-section of a stellar interior. One can see how modes of different angular degree penetrate the star at different depths.

How do we observe ν?

Review some work on solar-like oscillators and fundamental parameters.

1.4 Sampling Stellar Models

Typically, we start by producing a large grid of stellar models. Some are available online.

1.4.1 Grid-Based Modelling

What is GBM and give some examples e.g. BASTA Silva Aguirre, Davies, et al. (2015).

What is wrong with GBM?

1.4.2 Interpolation

Why Interpolation is useful?

How we might interpolate, e.g. linear ND interpolator example.

1.4.3 Machine Learning

A new alternative to GBM and interpolation is machine learning. Give examples of papers which have done this with stellar models.

Although ML stellar models is not new, it has not yet been applied to an HBM.

1.5 Observing Stars

How do we observe stars? E.g. how do we determine luminosity from parallax and magnitude.

How do we determine effective temperature from spectroscopy?

How do we determine metallicity?

1.5.1 Detecting Asteroseismic Oscillation Modes

Why do we care?

Name some missions which were able to detect asteroseismic oscillations and review their limitations.

Give an example from PBjam of detecting modes of oscillation.

Chapter 2

Hierarchically Modelling Many Stars

See the accompanying paper (Appendix A).

Chapter 3

Future Work

3.1 Including the Helium II Glitch

3.2 Increasing the Sample Size

3.3 To Higher Mass Stars and Beyond

Our next step is to include intermediate-mass stars with masses from approx. 1.2 solar masses to 3.0 solar masses.

References

Ahumada, Romina et al. (2019). "The Sixteenth Data Release of the Sloan Digital Sky Surveys: First Release from the APOGEE-2 Southern Survey and Full Release of eBOSS Spectra". In: *arXiv e-prints* 1912, arXiv:1912.02905.

Anderson, Lauren et al. (2018). "Improving Gaia Parallax Precision with a Data-Driven Model of Stars". In: *AJ* 156, p. 145. DOI: 10.3847/1538-3881/aad7bf.

Ando, H. and Y. Osaki (1975). "Nonadiabatic Nonradial Oscillations - an Application to the Five-Minute Oscillation of the Sun". In: *Publications of the Astronomical Society of Japan* 27, pp. 581–603.

Asplund, Martin et al. (2009). "The Chemical Composition of the Sun". In: *ARA&A* 47, pp. 481–522. DOI: 10.1146/annurev.astro.46.060407.145222.

Astropy Collaboration, A. M. Price-Whelan, et al. (2018). "The Astropy Project: Building an Open-Science Project and Status of the v2.0 Core Package". In: *AJ* 156, p. 123. DOI: 10.3847/1538-3881/aabc4f.

Astropy Collaboration, Thomas P. Robitaille, et al. (2013). "Astropy: A Community Python Package for Astronomy". In: *A&A* 558, A33. DOI: 10.1051/0004-6361/201322068.

Bahcall, John N. and Roger K. Ulrich (1988). "Solar Models, Neutrino Experiments, and Helioseismology". In: *Reviews of Modern Physics* 60, pp. 297–372. DOI: 10.1103/RevModPhys.60.297.

Balser, Dana S. (2006). "The Chemical Evolution of Helium". In: *AJ* 132, pp. 2326–2332. DOI: 10.1086/508515.

Barber, C. Bradford, David P. Dobkin, and Hannu Huhdanpaa (1996). "The Quickhull Algorithm for Convex Hulls". In: *ACM Trans. Math. Softw.* 22.4, pp. 469–483. DOI: 10.1145/235815.235821.

Bellinger, E. P. et al. (2019). "Stellar Ages, Masses, and Radii from Asteroseismic Modeling Are Robust to Systematic Errors in Spectroscopy". en. In: *A&A* 622, A130. DOI: 10.1051/0004-6361/201834461.

Berger, Travis A., Daniel Huber, Eric Gaidos, et al. (2018). "Revised Radii of *Kepler* Stars and Planets Using *Gaia* Data Release 2". en. In: *ApJ* 866.2, p. 99. DOI: 10.3847/1538-4357/aada83.

Berger, Travis A., Daniel Huber, Jennifer L. van Saders, et al. (2020). "The $Gaia$-$Kepler$ Stellar Properties Catalog I: Homogeneous Fundamental Properties for 186,000 $Kepler$ Stars". In: *arXiv e-prints* 2001, arXiv:2001.07737.

Bossini, D. et al. (2019). "Age Determination for 269 *Gaia* DR2 Open Clusters". en. In: *A&A* 623, A108. DOI: 10.1051/0004-6361/201834693.

Bovy, Jo et al. (2016). "On Galactic Density Modeling in the Presence of Dust Extinction". In: *ApJ* 818, p. 130. DOI: 10.3847/0004-637X/818/2/130.

Brogaard, K. et al. (2012). "Age and Helium Content of the Open Cluster NGC 6791 from Multiple Eclipsing Binary Members. II. Age Dependencies and New Insights". In: *Astronomy and Astrophysics* 543, A106. DOI: 10.1051/0004-6361/201219196.

Broomhall, A.-M. et al. (2011). "Solar-Cycle Variations of Large Frequency Separations of Acoustic Modes: Implications for Asteroseismology". In: *MNRAS* 413, pp. 2978–2986. DOI: 10.1111/j.1365-2966.2011.18375.x.

Campante, T. L. et al. (2016). "Spin-Orbit Alignment of Exoplanet Systems: Ensemble Analysis Using Asteroseismology". In: *ApJ* 819, p. 85. DOI: 10.3847/0004-637X/819/1/85.

Casagrande, Luca et al. (2007). "The Helium Abundance and ΔY/ΔZ in Lower Main-Sequence Stars". In: *MNRAS* 382, pp. 1516–1540. DOI: 10.1111/j.1365-2966.2007.12512.x.

Chan, Victor C. and Jo Bovy (2020). "The Gaia DR2 Parallax Zero-Point: Hierarchical Modelling of Red Clump Stars". In: *MNRAS* 493, pp. 4367–4381. DOI: 10.1093/mnras/staa571.

Chaplin, William J. and Andrea Miglio (2013). "Asteroseismology of Solar-Type and Red-Giant Stars". In: *Annual Review of Astronomy and Astrophysics* 51, pp. 353–392. DOI: 10.1146/annurev-astro-082812-140938.

Chiappini, C. et al. (2015). "Young [α /Fe]-Enhanced Stars Discovered by CoRoT and APOGEE: What Is Their Origin?" en. In: *A&A* 576, p. L12. DOI: 10.1051/0004-6361/201525865.

Chiosi, C. and F. M. Matteucci (1982). "The Helium to Heavy Element Enrichment Ratio, Delta Y/Delta Z". In: *A&A* 105, pp. 140–148.

Christensen-Dalsgaard, J. (1982). "Seismological Studies of the Sun and Other Stars". In: *Advances in Space Research* 2, pp. 11–19. DOI: 10.1016/0273-1177(82)90250-2.

— (1984). "What Will Asteroseismology Teach Us". In: p. 11.

Christensen-Dalsgaard, J. and D. O. Gough (1980). "Is the Sun Helium-Deficient". In: *Nature* 288, pp. 544–547. DOI: 10.1038/288544a0.

Clevert, Djork-Arné, Thomas Unterthiner, and Sepp Hochreiter (2015). "Fast and Accurate Deep Network Learning by Exponential Linear Units (ELUs)". In: *arXiv e-prints* 1511, arXiv:1511.07289.

Corsaro, E., J. De Ridder, and R. A. García (2015). "High-Precision Acoustic Helium Signatures in 18 Low-Mass Low-Luminosity Red Giants: Analysis from More than Four Years of *Kepler* Observations⋆". en. In: *A&A* 578, A76. DOI: 10.1051/0004-6361/201525922.

Das, Payel and Jason L. Sanders (2019). "MADE: A Spectroscopic Mass, Age, and Distance Estimator for Red Giant Stars with Bayesian Machine Learning". en. In: *Mon. Not. R. Astron. Soc.* 484, p. 294. DOI: 10.1093/mnras/sty2776.

Davies, G. R., V. Silva Aguirre, et al. (2016). "Oscillation Frequencies for 35 *Kepler* Solar-Type Planet-Hosting Stars Using Bayesian Techniques and Machine Learning". en. In: *MNRAS* 456.2, pp. 2183–2195. DOI: 10.1093/mnras/stv2593.

Davies, G. R., W. J. Chaplin, et al. (2015). "Asteroseismic Inference on Rotation, Gyrochronology and Planetary System Dynamics of 16 Cygni". In: *Monthly Notices of the Royal Astronomical Society* 446, pp. 2959–2966. DOI: 10.1093/mnras/stu2331.

Davies, G. R. and A. Miglio (2016). "Asteroseismology of Red Giants: From Analysing Light Curves to Estimating Ages". In: *Astronomische Nachrichten* 337, p. 774. DOI: 10.1002/asna.201612371.

Deubner, F.-L., R. K. Ulrich, and E. J. Rhodes Jr. (1979). "Solar P-Mode Oscillations as a Tracer of Radial Differential Rotation". In: *Astronomy and Astrophysics* 72, pp. 177–185.

Deubner, Franz-Ludwig and Douglas Gough (1984). "Helioseismology: Oscillations as a Diagnostic of the Solar Interior". In: *Annual Review of Astronomy and Astrophysics* 22, pp. 593–619. DOI: 10.1146/annurev.aa.22.090184.003113.

Eddington, A. S. (1926). *The Internal Constitution of the Stars*. Cambridge: Cambridge University Press.

Ferguson, Jason W. et al. (2005). "Low-Temperature Opacities". In: *The Astrophysical Journal* 623, pp. 585–596. DOI: 10.1086/428642.

Foreman-Mackey, Daniel et al. (2013). "Emcee: The MCMC Hammer". In: *Publications of the Astronomical Society of the Pacific* 125, p. 306. DOI: 10.1086/670067.

Frankel, Neige et al. (2020). "Keeping It Cool: Much Orbit Migration, yet Little Heating, in the Galactic Disk". In: *arXiv e-prints* 2002, arXiv:2002.04622.

Gaia Collaboration, A. G. A. Brown, et al. (2018). "Gaia Data Release 2. Summary of the Contents and Survey Properties". In: *Astronomy and Astrophysics* 616, A1. DOI: 10.1051/0004-6361/201833051.

Gaia Collaboration, T. Prusti, et al. (2016). "The Gaia Mission". In: *A&A* 595, A1. DOI: 10.1051/0004-6361/201629272.

Ginsburg, Adam et al. (2019). "Astroquery: An Astronomical Web-Querying Package in Python". In: *AJ* 157, p. 98. DOI: 10.3847/1538-3881/aafc33.

Glorot, Xavier, Antoine Bordes, and Y. Bengio (2011). "Deep Sparse Rectifier Neural Networks". In: *Proc. 14th Int. Conf. Artif. Intell. Statisitics AISTATS 2011* 15, pp. 315–323.

Goupil, MarieJo (2019). "Seismic Probe of Transport Processes in Red Giants". In: *ArXiv191009361 Astro-Ph*. arXiv: 1910.09361 [astro-ph].

Green, Gregory M. et al. (2019). "A 3D Dust Map Based on Gaia, Pan-STARRS 1, and 2MASS". In: *ApJ* 887, p. 93. DOI: 10.3847/1538-4357/ab5362.

Grevesse, N. and A. J. Sauval (1998). "Standard Solar Composition". In: *Space Sci. Rev.* 85, pp. 161–174. DOI: 10.1023/A:1005161325181.

Hahnloser, Richard H. R. et al. (2000). "Digital Selection and Analogue Amplification Coexist in a Cortex-Inspired Silicon Circuit". In: *Nature* 405, pp. 947–951. DOI: 10.1038/35016072.

Hall, Oliver J. et al. (2019). "Testing Asteroseismology with Gaia DR2: Hierarchical Models of the Red Clump". In: *MNRAS* 486, pp. 3569–3585. DOI: 10.1093/mnras/stz1092.

Hawkins, Keith et al. (2017). "Red Clump Stars and Gaia: Calibration of the Standard Candle Using a Hierarchical Probabilistic Model". In: *MNRAS* 471, pp. 722–729. DOI: 10.1093/mnras/stx1655.

Hekker, S. et al. (2012). "Solar-like Oscillations in Red Giants Observed with Kepler: Influence of Increased Timespan on Global Oscillation Parameters". In: *Astronomy and Astrophysics* 544, A90. DOI: 10.1051/0004-6361/201219328.

Hendriks, L. and C. Aerts (2019). "Deep Learning Applied to the Asteroseismic Modeling of Stars with Coherent Oscillation Modes". In: *PASP* 131, p. 108001. DOI: 10.1088/1538-3873/aaeeec.

Hogg, David W. (2012). "Data Analysis Recipes: Probability Calculus for Inference". In: *arXiv e-prints* 1205, arXiv:1205.4446.

Hogg, David W., Jo Bovy, and Dustin Lang (2010). "Data Analysis Recipes: Fitting a Model to Data". In: *arXiv e-prints* 1008, arXiv:1008.4686.

Hogg, David W. and Daniel Foreman-Mackey (2018). "Data Analysis Recipes: Using Markov Chain Monte Carlo". In: *ApJS* 236, p. 11. DOI: 10.3847/1538-4365/aab76e.

Hogg, David W., Adam D. Myers, and Jo Bovy (2010). "Inferring the Eccentricity Distribution". In: *ApJ* 725, pp. 2166–2175. DOI: 10.1088/0004-637X/725/2/2166.

Hon, Marc, Dennis Stello, and Jie Yu (2017). "Deep Learning Classification in Asteroseismology". en. In: *Mon. Not. R. Astron. Soc.* 469.4, pp. 4578–4583. DOI: 10.1093/mnras/stx1174.

Hon, Marc, Dennis Stello, and Joel C. Zinn (2018). "Detecting Solar-like Oscillations in Red Giants with Deep Learning". en. In: *ApJ* 859.1, p. 64. DOI: 10.3847/1538-4357/aabfdb.

Howe, Rachel et al. (2020). "Solar Cycle Variation of Nmax in Helioseismic Data and Its Implications for Asteroseismology". In: *MNRAS* 493, pp. L49–L53. DOI: 10.1093/mnrasl/slaa006.

Huber, D., T. R. Bedding, et al. (2011). "Testing Scaling Relations for Solar-like Oscillations from the Main Sequence to Red Giants Using Kepler Data". In: *ApJ* 743, p. 143. DOI: 10.1088/0004-637X/743/2/143.

Huber, D., D. Stello, et al. (2009). "Automated Extraction of Oscillation Parameters for Kepler Observations of Solar-Type Stars". In: *Communications in Asteroseismology* 160, p. 74.

Kahn, F. D. (1961). "Sound Waves Trapped in the Solar Atmosphere." In: *The Astrophysical Journal* 134, p. 343. DOI: 10.1086/147164.

Kinemuchi, K. et al. (2012). "Demystifying Kepler Data: A Primer for Systematic Artifact Mitigation". In: *Publications of the Astronomical Society of the Pacific* 124, p. 963. DOI: 10.1086/667603.

Kingma, Diederik P. and Jimmy Ba (2014). "Adam: A Method for Stochastic Optimization". In: *arXiv e-prints* 1412, arXiv:1412.6980.

Kjeldsen, H. and T. R. Bedding (1995). "Amplitudes of Stellar Oscillations: The Implications for Asteroseismology." In: *Astronomy and Astrophysics* 293, pp. 87–106.

Kuszlewicz, James S. et al. (2019). "Bayesian Hierarchical Inference of Asteroseismic Inclination Angles". In: *MNRAS* 488, pp. 572–589. DOI: 10.1093/mnras/stz1689.

Lebreton, Y., M.J. Goupil, and J. Montalbán (2014). "How Accurate Are Stellar Ages Based on Stellar Models?: I. The Impact of Stellar Models Uncertainties". en. In: *EAS Publications*

Series 65. Ed. by Y. Lebreton, D. Valls-Gabaud, and C. Charbonnel, pp. 99–176. DOI: 10.1051/eas/1465004.

Leistedt, Boris and David W. Hogg (2017). "Hierarchical Probabilistic Inference of the Color-Magnitude Diagram and Shrinkage of Stellar Distance Uncertainties". In: *AJ* 154, p. 222. DOI: 10.3847/1538-3881/aa91d5.

Licquia, Timothy C. and Jeffrey A. Newman (2015). "Improved Estimates of the Milky Way's Stellar Mass and Star Formation Rate from Hierarchical Bayesian Meta-Analysis". In: *ApJ* 806, p. 96. DOI: 10.1088/0004-637X/806/1/96.

Lightkurve Collaboration et al. (2018). "Lightkurve: Kepler and TESS Time Series Analysis in Python". In: *Astrophysics Source Code Library*, ascl:1812.013.

Lindegren, L. et al. (2018). "Gaia Data Release 2. The Astrometric Solution". In: *A&A* 616, A2. DOI: 10.1051/0004-6361/201832727.

Lomb, N. R. (1976). "Least-Squares Frequency Analysis of Unequally Spaced Data". In: *Astrophysics and Space Science* 39, pp. 447–462. DOI: 10.1007/BF00648343.

Magic, Z., A. Weiss, and M. Asplund (2015). "The Stagger-Grid: A Grid of 3D Stellar Atmosphere Models. III. The Relation to Mixing Length Convection Theory". In: *A&A* 573, A89. DOI: 10.1051/0004-6361/201423760.

Martinez, Gregory D. (2015). "A Robust Determination of Milky Way Satellite Properties Using Hierarchical Mass Modelling". In: *MNRAS* 451, pp. 2524–2535. DOI: 10.1093/mnras/stv942.

Morton, Timothy D. (2015). "Isochrones: Stellar Model Grid Package". In: *Astrophys. Source Code Libr.* ascl:1503.010.

Morton, Timothy D. and Joshua N. Winn (2014). "Obliquities of Kepler Stars: Comparison of Single- and Multiple-Transit Systems". In: *ApJ* 796, p. 47. DOI: 10.1088/0004-637X/796/1/47.

Mosser, B. et al. (2015). "Period Spacings in Red Giants. I. Disentangling Rotation and Revealing Core Structure Discontinuities". In: *Astronomy and Astrophysics* 584, A50. DOI: 10.1051/0004-6361/201527075.

Nissen, P. E. et al. (2017). "High-Precision Abundances of Elements in Kepler LEGACY Stars. Verification of Trends with Stellar Age". In: *Astronomy and Astrophysics* 608, A112. DOI: 10.1051/0004-6361/201731845.

Ohn, Ilsang and Yongdai Kim (2019). "Smooth Function Approximation by Deep Neural Networks with General Activation Functions". In: *Entropy* 21.7, p. 627. DOI: 10.3390/e21070627. arXiv: 1906.06903.

Paxton, Bill, Lars Bildsten, et al. (2011). "Modules for Experiments in Stellar Astrophysics (MESA)". In: *ApJS* 192, p. 3. DOI: 10.1088/0067-0049/192/1/3.

Paxton, Bill, Matteo Cantiello, et al. (2013). "Modules for Experiments in Stellar Astrophysics (MESA): Planets, Oscillations, Rotation, and Massive Stars". In: *The Astrophysical Journal Supplement Series* 208, p. 4. DOI: 10.1088/0067-0049/208/1/4.

Paxton, Bill, Pablo Marchant, et al. (2015). "Modules for Experiments in Stellar Astrophysics (MESA): Binaries, Pulsations, and Explosions". In: *The Astrophysical Journal Supplement Series* 220, p. 15. DOI: 10.1088/0067-0049/220/1/15.

Paxton, Bill, Josiah Schwab, et al. (2018). "Modules for Experiments in Stellar Astrophysics (MESA): Convective Boundaries, Element Diffusion, and Massive Star Explosions". In: *The Astrophysical Journal Supplement Series* 234, p. 34. DOI: 10.3847/1538-4365/aaa5a8.

Paxton, Bill, R. Smolec, et al. (2019). "Modules for Experiments in Stellar Astrophysics (MESA): Pulsating Variable Stars, Rotation, Convective Boundaries, and Energy Conservation". In: *The Astrophysical Journal Supplement Series* 243, p. 10. DOI: 10.3847/1538-4365/ab2241.

Pinsonneault, Marc H. et al. (2012). "A Revised Effective Temperature Scale for the Kepler Input Catalog". In: *ApJS* 199, p. 30. DOI: 10.1088/0067-0049/199/2/30.

Qian, Ning (1999). "On the Momentum Term in Gradient Descent Learning Algorithms". en. In: *Neural Networks* 12.1, pp. 145–151. DOI: 10.1016/S0893-6080(98)00116-6.

Ramachandran, Prajit, Barret Zoph, and Quoc V. Le (2017). "Searching for Activation Functions". In: *arXiv e-prints* 1710, arXiv:1710.05941.

Reese, D. R. et al. (2016). "SpaceInn Hare-and-Hounds Exercise: Estimation of Stellar Properties Using Space-Based Asteroseismic Data". In: *A&A* 592, A14. DOI: 10.1051/0004-6361/201527987.

Ribas, Ignasi et al. (2000). "Chemical Composition of Eclipsing Binaries: A New Approach to the Helium-to-Metal Enrichment Ratio". In: *MNRAS* 313, pp. 99–111. DOI: 10.1046/j.1365-8711.2000.03195.x.

Rogers, F. J. and A. Nayfonov (2002). "Updated and Expanded OPAL Equation-of-State Tables: Implications for Helioseismology". In: *The Astrophysical Journal* 576, pp. 1064–1074. DOI: 10.1086/341894.

Rogers, Leslie A. (2015). "Most 1.6 Earth-Radius Planets Are Not Rocky". In: *ApJ* 801, p. 41. DOI: 10.1088/0004-637X/801/1/41.

Ruder, Sebastian (2016). "An Overview of Gradient Descent Optimization Algorithms". In: *arXiv e-prints* 1609, arXiv:1609.04747.

Salvatier, John, Thomas V. Wiecki, and Christopher Fonnesbeck (2016). "Probabilistic Programming in Python Using PyMC3". en. In: *PeerJ Comput. Sci.* 2, e55. DOI: 10.7717/peerj-cs.55.

Sandquist, Eric L. et al. (2020). "Variability in the Massive Open Cluster NGC 1817 from K2: A Rich Population of Asteroseismic Red Clump, Eclipsing Binary, and Main Sequence Pulsating Stars". In: *ArXiv200101839 Astro-Ph*. arXiv: 2001.01839 [astro-ph].

Scargle, J. D. (1982). "Studies in Astronomical Time Series Analysis. II - Statistical Aspects of Spectral Analysis of Unevenly Spaced Data". In: *The Astrophysical Journal* 263, pp. 835–853. DOI: 10.1086/160554.

Serenelli, Aldo M. and Sarbani Basu (2010). "Determining the Initial Helium Abundance of the Sun". In: *ApJ* 719, pp. 865–872. DOI: 10.1088/0004-637X/719/1/865.

Serenelli, Aldo, Jennifer Johnson, et al. (2017). "The First APOKASC Catalog of Kepler Dwarf and Subgiant Stars". In: *ApJS* 233, p. 23. DOI: 10.3847/1538-4365/aa97df.

Si, Shijing et al. (2017). "A Hierarchical Model for the Ages of Galactic Halo White Dwarfs". In: *MNRAS* 468, pp. 4374–4388. DOI: 10.1093/mnras/stx765.

Silva Aguirre, V., G. R. Davies, et al. (2015). "Ages and Fundamental Properties of Kepler Exoplanet Host Stars from Asteroseismology". en. In: *MNRAS* 452.2, p. 2127. DOI: 10.1093/mnras/stv1388.

Silva Aguirre, Víctor, Mikkel N. Lund, et al. (2017). "Standing on the Shoulders of Dwarfs: The Kepler Asteroseismic LEGACY Sample. II.Radii, Masses, and Ages". In: *ApJ* 835, p. 173. DOI: 10.3847/1538-4357/835/2/173.

Smith, Jeffrey C. et al. (2012). "Kepler Presearch Data Conditioning II - A Bayesian Approach to Systematic Error Correction". In: *Publications of the Astronomical Society of the Pacific* 124, p. 1000. DOI: 10.1086/667697.

Soderblom, David R. (2010). "The Ages of Stars". en. In: *ARA&A* 48.1, pp. 581–629. DOI: 10.1146/annurev-astro-081309-130806.

Soni, Harsh et al. (2020). "Phases and Excitations of Active Rod-Bead Mixtures: Simulations and Experiments". In: *ArXiv200100173 Cond-Mat*. arXiv: 2001.00173 [cond-mat].

Stumpe, Martin C. et al. (2012). "Kepler Presearch Data Conditioning I—Architecture and Algorithms for Error Correction in Kepler Light Curves". In: *Publications of the Astronomical Society of the Pacific* 124, p. 985. DOI: 10.1086/667698.

Sutskever, Ilya et al. (2013). "On the Importance of Initialization and Momentum in Deep Learning". In: ed. by Sanjoy Dasgupta and David McAllester. Vol. 28. Proceedings of Machine Learning Research. Atlanta, Georgia, USA: PMLR, pp. 1139–1147.

Townsend, R. H. D. and S. A. Teitler (2013). "GYRE: An Open-Source Stellar Oscillation Code Based on a New Magnus Multiple Shooting Scheme". In: *Monthly Notices of the Royal Astronomical Society* 435, pp. 3406–3418. DOI: 10.1093/mnras/stt1533.

Trampedach, Regner et al. (2014). "Improvements to Stellar Structure Models, Based on a Grid of 3D Convection Simulations - II. Calibrating the Mixing-Length Formulation". In: *MNRAS* 445, pp. 4366–4384. DOI: 10.1093/mnras/stu2084.

Ulrich, R. K. (1986). "Determination of Stellar Ages from Asteroseismology". In: *The Astrophysical Journal Letters* 306, pp. L37–L40. DOI: 10.1086/184700.

Ulrich, Roger K. (1970). "The Five-Minute Oscillations on the Solar Surface". In: *The Astrophysical Journal* 162, p. 993. DOI: 10.1086/150731.

VanderPlas, Jacob T. (2018). "Understanding the Lomb-Scargle Periodogram". In: *The Astrophysical Journal Supplement Series* 236, p. 16. DOI: 10.3847/1538-4365/aab766.

Verma, Kuldeep, Shravan Hanasoge, et al. (2016). "Asteroseismic Determination of Fundamental Parameters of Sun-like Stars Using Multilayered Neural Networks". In: *MNRAS* 461, pp. 4206–4214. DOI: 10.1093/mnras/stw1621.

Verma, Kuldeep, Keyuri Raodeo, et al. (2019). "Helium Abundance in a Sample of Cool Stars: Measurements from Asteroseismology". In: *MNRAS* 483, pp. 4678–4694. DOI: 10.1093/mnras/sty3374.

Viani, Lucas S. et al. (2018). "Investigating the Metallicity-Mixing-Length Relation". In: *The Astrophysical Journal* 858, p. 28. DOI: 10.3847/1538-4357/aab7eb.

von Hippel, Ted et al. (2006). "Inverting Color-Magnitude Diagrams to Access Precise Star Cluster Parameters: A Bayesian Approach". en. In: *ApJ* 645.2, pp. 1436–1447. DOI: 10.1086/504369.

Vrard, M. et al. (2015). "Helium Signature in Red Giant Oscillation Patterns Observed by *Kepler*". en. In: *A&A* 579, A84. DOI: 10.1051/0004-6361/201425064.

White, Timothy R. et al. (2011). "Calculating Asteroseismic Diagrams for Solar-like Oscillations". In: *The Astrophysical Journal* 743, p. 161. DOI: 10.1088/0004-637X/743/2/161.

Zinn, Joel C., Marc H. Pinsonneault, Daniel Huber, and Dennis Stello (2019). "Confirmation of the Gaia DR2 Parallax Zero-Point Offset Using Asteroseismology and Spectroscopy in the Kepler Field". In: *ApJ* 878, p. 136. DOI: 10.3847/1538-4357/ab1f66.

Zinn, Joel C., Marc H. Pinsonneault, Daniel Huber, Dennis Stello, et al. (2019). "Testing the Radius Scaling Relation with Gaia DR2 in the Kepler Field". In: *ApJ* 885, p. 166. DOI: 10.3847/1538-4357/ab44a9.

Appendix A

Accompanying Paper

MNRAS **000**, 1–8 (2020) Preprint 14 September 2020 Compiled using MNRAS LATEX style file v3.0

TBC: Hierarchically modelling *Kepler* dwarfs using machine learning to uncover helium enrichment in the solar neighbourhood

Alexander J. Lyttle,[1,2]★ Tanda Li,[1,2] Guy R. Davies,[1,2] Lindsey M. Carboneau[1,2] and TBC
[1]*School of Physics and Astronomy, University of Birmingham, Birmingham, B15 2TT, UK*
[2]*Stellar Astrophysics Centre (SAC), Department of Physics and Astronomy, Aarhus University, Ny Munkegade 120, DK-8000 Aarhus C, Denmark*

Accepted XXX. Received YYY; in original form ZZZ

ABSTRACT

Key words:
asteroseismology – methods: miscellaneous – methods: statistical – stars: fundamental parameters – stars: low-mass

1 INTRODUCTION

Motivation - precise and accurate stellar fundamentals. Useful for e.g. galactic archaeology and exoplanet research.

Audience - astrophysicist with some knowledge Introduce new method and reference Guy's paper:

- Summarise the typical way in which stellar fundamentals are estimated and their pitfalls (e.g. discrete sampling, and assuming solar calibrated mixing-length parameter and helium enrichment)
  - Problems with grid-based-modelling (e.g. proper sampling)
  - assuming fixed DYDZ and MLT bad; attempts to interpolate, slow and hard to scale
- Why hierarchical models are good with examples of HBMs in astrophysics
- Advantage of HBM is to incorporate population-level distributions
- Why HBMs are difficult with stellar models.
- Introduce the neural network as a way to overcome these issues and give examples of neural networks to approximate models in astrophysics
- Highlight the novel element of this paper - the first application of combining a neural network emulator with a hierarchical model to provide shrinkage of fundamentals uncertainties and simultaneously study a helium enrichment relation
- Use a helium enrichment law prior, and assume a distribution of mixing-length of the population-level, to inform object-level parameters

Why do we care about helium and mixing-length? These parameters have a large (be quantitative) affect on stellar ages. Good stellar ages allow us to better study galactic archaeology (with citations).

Given that we are assuming a helium enrichment prior, give a brief summary of research into the helium enrichment and typical values for $\Delta Y/\Delta Z$. Note that in reality there may not be a linear law, and more may be studied in future work (or using a GP like in Guy's paper?). Why do we care about an enrichment law? Why is it physically justified?

Given that we are assuming a mixing-length distribution, mention this is mainly a nuisance parameter which we will marginalize over, since this differs depending on model physics. However, later justify a normal spread by referring to work (e.g. Magic) which shows little variation in the area of the HRD we are studying.

Outline the structure of the work. We are demonstrating the method on an asteroseismic sample of dwarfs and subgiants from Serenelli 2017. We first introduce the data and why we choose to use spectroscopy and asteroseismology. We then introduce the method, from the grid of stellar models

Why asteroseismology and why this particular set of Kepler-field dwarfs? Acknowledge selection bias but explain that with TESS providing an all-sky sample of solar-like oscillators this method can be extended to a much larger sample size.

Note: here is an example of a paper which would benefit from a value of the intrinsic spread in helium enrichment: (Zinn et al. 2019) 'Until such a time as the intrinsic scatter in helium enrichment can be determined, which... hinders a comparison between the theoretical metallicity trend and the observed radius agreement... the asteroseismic scaling relation radius does not require a metallicity term...'. In other words, they assume a helium enrichment law but this hinders their ability to study the seismic scaling relation correction.

2 DATA

We began with the sample of 415 stars from the first APOKASC catalogue of dwarfs and subgiants (S17). It is, to date, the most comprehensive sample of asteroseismic dwarfs and subgiant stars observed by the *Kepler* mission. We adopted the global asteroseismic parameters – the large frequency separation, $\Delta\nu$, and the

★ E-mail: ajl573@student.bham.ac.uk

frequency of maximum power, $\nu_{\rm max}$ – determined by S17, and references therein. We then cross matched the sample with *Gaia* Data Release 2 for high-precision parallaxes, and the Apache Point Observatory Galaxy Evolution Experiment (APOGEE) catalogue to obtain spectroscopic metallicities and effective temperatures. Using the cross matched catalogue, we calculated luminosities for the full sample with Two-Micron All Sky Survey (2MASS) photometry and selected a subsample of stars with similar metallicities and masses. Our method is described in detail in the remainder of this section.

We cross matched the *Kepler* input catalogue (KIC) for the sample with the *Gaia* DR2 catalogue taking the nearest neighbours within a 4" radius [CITE GAIA]. All but two of the sample of 415 stars were available. We then adopted the *Gaia* parallaxes, assuming a zero-point offset of 0.05 mas in the sense that the *Gaia* parallaxes are underestimated. We chose this value in line with recent studies on the *Gaia* zero-point parallax offset in the *Kepler* field [CITATIONS].

We adopted spectroscopic metallicities, [M/H], and effective temperatures, $T_{\rm eff}$determined by the APOGEE stellar parameters and chemical abundances pipeline (ASPCAP) from the second data release of the fourth phase of the Sloan Digital Sky Survey (SDSS) otherwise known as Data Release 14 (DR14). We cross matched the APOGEE DR14 catalogue with our *Kepler-Gaia* DR2 cross match yielding spectroscopic parameters for all 413 stars in the sample.

In order to remove more evolved stars, we made a cut in surface gravity, g. We used asteroseismic $\nu_{\rm max}$ with ASPCAP $T_{\rm eff}$ and rearranged the asteroseismic scaling relation to get,

$$\log g \approx \log g_{\odot} + \log\left(\frac{\nu_{\rm max}}{\nu_{\rm max,\odot}}\right) - \frac{1}{2}\log\left(\frac{T_{\rm eff}}{T_{\rm eff,\odot}}\right), \quad (1)$$

where solar reference values of $\nu_{\rm max,\odot} = 3090 \pm 30\,\mu$Hz (Huber et al. 2011) $\log g_{\odot} = 4.44$ dex and $T_{\rm eff,\odot} = 5777$ K were used to determine the log surface gravity, $\log g$.

We determined luminosities for the sample using the direct method of ISOCLASSIFY [CITE HUBER]. We calculated absolute K_S-band magnitudes using K_s-band photometry from the 2MASS, distances from the zero-point-offset-corrected parallaxes from *Gaia* DR2 and extinctions determined from the 3D galactic reddening maps of Green et al. (2019) [CITE]. We then determined absolute bolometric magnitudes by interpolating the MIST bolometric correction tables using ASPCAP [M/H]and $T_{\rm eff}$, asteroseismic $\log g$ and absolute magnitude as inputs. An uncertainty of 0.02 mag was assumed for both the extinctions and bolometric corrections, in line with typical uncertainties from randomly sampling the input data within their errors. The resulting distances, absolute magnitudes and luminosities with their respective uncertainties are given in Table X.

We selected a subset from the above sample which we determined to lie within the bounds of the model grid described in Section 3.1 using mass estimates from S17. We determined such "on-grid" stars where their estimated mass and metallicity were within one standard deviation of the grid boundary, from 0.8 to 1.2 $M_{\odot}$ in mass and from −0.5 to 0.5 dex in metallicity. We also cut targets in the sample with an asteroseimic $\log g$ less than 3.8 dex to remove more evolved stars. The cut in mass was motivated by our choice of model physics described in Section 3.1. Stars with $M \gtrsim 1.15\,M_{\odot}$ are understood to have a convective, hydrogen-burning core, with some dependence on the choice of stellar physics [CITE Appourchaux](). Modelling stars with a convective core requires the consideration of extra mixing due to the overshooting of convective cells at the core boundary [CITE OVERSHOOT PAPERS], which is beyond the scope of this work.

The final sample comprised 81 stars, after removing stars with null observables. The data for 10 stars from the sample is shown in Table 1 and the full table may downloaded LINK. The Hertzsprung-Rusell diagram in Figure **??** shows the sample plot above a selection of stellar evolutionary tracks from the grid described in Section 3.1. A second plot shows the sample in context with a selection of *Kepler* solar neighbourhood stars. Consider the range of parallaxes plot when defininging the solar neighbourhood (less that 1 kpc).

3 METHODS

We base our methods on that of Davies et al. (in prep.). In the following sections, we first describe the grid of stellar evolutionary models (Section 3.1). We then describe the artificial neural network (ANN) which we trained on the gird in Section 3.2. Finally, we describe the three statistic models we developed to test and compare our new method with the results of S17.

3.1 Grid of stellar models

We built up a stellar model grid to train the NN model. The gird includes four independent model inputs: stellar mass (M), initial helium fraction ($Y_{\rm init}$), initial metallicity ([Fe/H]), and the mixing-length parameter ($\alpha_{\rm MLT}$). Ranges and grid steps of the four model inputs are summarised in Table 2. We computed each stellar evolutionary track from the Hayashi line and to the base of red-giant branch where $\log g = 3.6$ dex. We also computed 4,000 evolutionary tracks with random input values in the parameter space for validating the results.

3.1.1 *Stellar models and input physics*

We used Modules for Experiments in Stellar Astrophysics (MESA, version 12115) to establish a grid of stellar models. MESA is an open-source stellar evolution package which is undergoing active development. Descriptions of input physics and numerical methods can be found in Paxton et al. (2011, 2013, 2015). We adopted the solar chemical mixture [$(Z/X)_{\odot} = 0.0181$] provided by Asplund et al. (2009). The initial chemical composition was calculated by:

$$\log(Z_{\rm init}/X_{\rm init}) = \log(Z/X)_{\odot} + [{\rm Fe/H}]. \quad (2)$$

We used the MESA $\rho - T$ tables based on the 2005 update of OPAL EOS tables (Rogers & Nayfonov 2002) and OPAL opacity supplemented by low-temperature opacity (Ferguson et al. 2005). The MESA 'simple' photosphere were used as the set of boundary conditions for modelling the atmosphere. The mixing-length theory of convection was implemented, where $\alpha_{\rm MLT} = \ell_{\rm MLT}/H_p$ is the mixing-length parameter. We also applied the MESA predictive mixing scheme (Paxton et al. 2018, 2019) in the model computation.

The evolution time step was mainly controlled by the set-up tolerances on changes in surface effective temperature and luminosity. We saved one structural model at every time step at main sequence and every two steps after central hydrogen exhaustion. For each evolutionary track, we obtained ∼100 at the main-sequence stage and 500 – 700 at evolved stages.

Table 1.

Name	$T_{\rm eff}$ (K)	$\sigma_{T_{\rm eff}}$ (K)	L ($L_\odot$)	σ_L ($L_\odot$)	$\Delta\nu$ (μHz)	$\sigma_{\Delta\nu}$ (μHz)	[M/H] (dex)	$\sigma_{\rm [M/H]}$ (dex)	log g (dex)	$\sigma_{\log g}$ (dex)
KIC10079226	5928.84	124.84	1.57	0.05	116.04	0.73	0.16	0.07	4.36	0.01
KIC10215584	5666.92	119.33	1.64	0.06	115.16	2.83	0.04	0.07	4.27	0.09
KIC10319352	5456.17	106.65	1.85	0.06	78.75	1.73	0.27	0.06	3.96	0.13
KIC10322381	6146.79	148.58	2.44	0.08	86.64	6.57	-0.32	0.08	4.19	0.04
KIC10417911	5628.26	109.99	3.41	0.12	56.14	2.10	0.34	0.07	3.94	0.02
KIC10732098	5669.65	119.28	3.02	0.12	62.18	1.92	0.05	0.07	3.96	0.02
KIC10794845	6035.12	140.46	1.64	0.06	116.35	6.70	-0.21	0.08	4.40	0.11
KIC10963065	6039.78	139.10	1.88	0.06	103.21	0.11	-0.16	0.08	4.30	0.01
KIC10971974	5748.00	142.40	1.43	0.05	106.63	3.31	-0.07	0.09	4.32	0.04
KIC11021413	5329.18	102.98	3.16	0.11	48.16	1.29	0.01	0.04	3.84	0.01

Table 2. Stellar model computations for training and test datasets.

Training model set (Grid-based)			
Input Parameter	Range	Increment	$N_{\rm track}$
M [$M_\odot$]	0.80 – 1.20	0.01	
[Fe/H] [dex]	-0.5 – 0.2/0.2 – 0.5	0.1/0.05	15,375
$Y_{\rm init}$	0.24 – 0.32	0.02	
$\alpha_{\rm MLT}$	1.7 – 2.5	0.2	

3.1.2 Oscillation models and seismic $\Delta\nu$

Theoretical stellar oscillations were calculated with the GYRE code (version 5.1), which was developed by Townsend & Teitler (2013). And we computed radial modes (for $\ell = 0$) by solving the adiabatic stellar pulsation equations with the structural models generated by MESA. We computed a seismic large separation($\Delta\nu$) for each model with theoretical radial modes to avoid the systematic offset of the scaling relation. We derived $\Delta\nu$ with the approach given by White et al. (2011), which is a weighted least-squares fit to the radial frequencies as a function of n.

3.2 Artificial neural network

Once we constructed our grid of models, we needed a way in which we could continuously sample the grid for use in our statistical model. We could interpolate the grid, as is common in the isochrone-fitting method [CITE], but this would be slow due to the high dimensionality of our inputs and the size of the dataset. Moreover, evaluating the gradient of an interpolated function is difficult [IMPOSSIBLE?]. In this work, we utilise deep learning (DL) to approximate the grid of stellar models via an artificial neural network (ANN). The ANN is advantageous over interpolation due to scaling well with dimensionality, fast training and evaluation, and easy gradient evaluation due to its roots in linear algebra [CITE].

We trained an ANN on the data generated by the grid of stellar models to map fundamentals to observables. Firstly, we split the grid of models into a *train* and *test* dataset for tuning the ANN, as described in Section 3.2.1. We then tested a multitude of ANN configurations and training data augmentations, evaluating them with the test dataset in Section 3.2.2. Finally, in Section 3.2.3, we reserved a randomly generated set of stellar models as our final *validation* dataset to evaluate the approximation ability of the best-performing ANN. In this section, we briefly describe the theory and motivation behind the ANN.

An ANN is a network of artificial *neurons* which each transform some input vector, $\boldsymbol{x}$ based on trainable weights, $\boldsymbol{w}$ and a bias, b [CITATIONS]. The weights are represented by the connections between neurons and the bias is a unique scalar associated with each neuron. Deep learning (DL) is the name given to the case where neurons are arranged into a series of layers such that any neuron in layer $k-1$ is connected to at least one of the neurons in layer k.

In this work, we considered a fully-connected ANN, where each neuron in layer $k-1$ is connected to every neuron in layer k. The output of a given neuron, i in layer k is,

$$x_{i,k} = f_k(\boldsymbol{w}_{i,k} \cdot \boldsymbol{x}_{k-1} + b_{i,k}) \tag{3}$$

where f_k is the *activation* function for the k-th layer, $\boldsymbol{w}_{i,k}$ are the weights connecting all the neurons in layer $k-1$ to the current neuron, and $b_{i,k}$ is the bias. This generalises such that the output of the k-th layer is,

$$\boldsymbol{x}_k = f_k(\boldsymbol{W}_k \cdot \boldsymbol{x}_{k-1} + \boldsymbol{b}_k), \tag{4}$$

where $\boldsymbol{W}_k$ is the matrix of weights leading to all neurons in the k-th layer. For a regression neural network, we typically have a linear activation function applied to the output of the final layer. Therefore, the output of a network of M hidden layers with initial input X is,

$$\boldsymbol{Y} = \boldsymbol{W}_M \cdot f_{M-1}(\dots f_1(\boldsymbol{W}_1 \cdot f_0(\boldsymbol{W}_0 \cdot \boldsymbol{X} + \boldsymbol{b}_0) + \boldsymbol{b}_1)) + \boldsymbol{b}_M \tag{5}$$

We also restricted our configuration to an ANN with the same number of neurons, N in each hidden layer. Hereafter, we refer to our choice of neurons per layer, N and hidden layers, M as the *architecture*.

To fit the ANN, we used a set of training data, $\boldsymbol{D}_{\rm train} = \{(\boldsymbol{X}_1, \boldsymbol{Y}_1) \dots (\boldsymbol{X}_{N_{\rm train}}, \boldsymbol{Y}_{N_{\rm train}})\}$ comprising $N_{\rm train}$ input-output pairs. We split the training data into pseudo-random batches, $\boldsymbol{D}_{\rm batch}$ because this has been shown to improve model convergence and computational efficiency [CITE]. The set of predictions made for each batch is evaluated with an error function, $E(\boldsymbol{D}_{\rm batch})$, also known as the *loss* which quantifies the difference between the training data and predictions. We also considered an addition to the loss called *regularisation* which helps reduce over-fitting (CITE). During fitting, the weights are updated after each batch using an algorithm called the *optimizer*, back-propagating the error with the goal of minimising the loss.

We varied the architecture, number of batches, choice of

loss function, optimizer and regularisation during the optimisation phase. For each set of ANN parameters, we initialised the ANN with a random set of weights and biases and minimized the loss over a given number of *epochs*. An epoch is defined as one iteration through the entire training dataset, $\boldsymbol{D}$)train. We tracked the loss for each ANN using an independent test dataset to determine the most effective choice of ANN parameters (see Section 3.2.2).

3.2.1 *Training data*

To form the training dataset, we pseudo-randomly sampled 7.736×10^6 points from the grid of stellar models, with the remaining $\sim 2 \times 10^6$ points given to the test dataset. Before we trained a given ANN architecture, we standardised the training dataset by subtracting the median, $\mu_{1/2}$ and dividing by the standard deviation, σ. We show the locations and scales of the standardisation for each parameter in Table A1.

We produced a validation dataset of $\sim 2 \times 10^6$ stellar models evolvoved using MESA with randomly generated initial mass, metallicity, helium and mixing-length-theory parameter. This dataset was set aside and evaluated on the final ANN.

During initial tuning, we found that having stellar age as an input was unstable, because it varied heavily with the other input parameters. We mitigated this by introducing an input to describe the fraction of time a star has spent in a given evolutionary phase, $f_{\rm evol}$.

$$f_{\rm evol} = \begin{cases} f_{\rm MS}, & f_{\rm MS} \leq 1 \\ 1 + \frac{\tau - \tau_{\rm MS}}{\tau_{\log g=3.6} - \tau_{\rm MS}}, & f_{\rm MS} > 1 \end{cases} \quad (6)$$

where $\tau_{\log g=3.6}$ is the age of the star at the end of the track,

$$f_{\rm MS} = \frac{\tau}{\tau_{\rm MS}}, \quad (7)$$

and $\tau_{\rm MS}$ is the main sequence lifetime, defined in the models as the point where the central hydrogen fraction, $X_c < 0.XX$. In other words, a star with $f_{\rm evol} \in (0, 1]$ is in its main sequence phase, burning hydrogen in its core, and $f_{\rm evol} \in (1, 2]$ has left the main sequence and began burning hydrogen in a shell. By proxy, $f_{\rm evol}$ gives the ANN information about the internal state of the star which effects the output observables. Otherwise, $f_{\rm evol}$ is a meaningless parameter, although it could loosely be interpreted as a measure of the evolutionary phase of the star.

We also observed the ANN struggled to fit areas with a high rate of change in observables. To bias training to such areas, we calculated the gradient in $T_{\rm eff}$ and $\log g$ between each point for each stellar evolutionary track and used them as optional weights in the loss during tuning.

After preliminary tuning, we chose the ANN input and output parameters to be $\boldsymbol{X} = \{f_{\rm evol}, M, \alpha_{\rm mlt}, Y_{\rm init}, Z_{\rm init}\}$ and $\boldsymbol{Y} = \{\log(\tau), T_{\rm eff}, R, \Delta\nu, [{\rm M/H}]_{\rm surf}\}$ respectively. The inputs correspond to initial conditions in the stellar modelling code and the outputs correspond to surface conditions throughout its lifetime, with the exception of age which is mapped from $f_{\rm evol}$. A generalised form of the neural network is depicted in Figure 1.

3.2.2 *Tuning*

We tuned the ANN parameters by varying them in both a grid-based and heuristic approach.

We evaluated the performance of three activation functions: the hyperbolic-tangent, the rectified linear unit (ReLU; Hahnloser et al. 2000; Glorot et al. 2011) and the exponential linear unit (ELU; Clevert et al. 2015). Although the ReLU activation function outperformed the other two in speed and accuracy, the ANN output was not smooth. The discontinuity in the ReLU function, $f(x) = \max(0, x)$ caused the output to also be discontinuous. This made the ANN difficult to sample with a gradient-based sampler such as the Hamiltonian Monte-Carlo (HMC) method. Out of the remaining activation functions, ELU performed the best, providing a smooth output which was well-suited to our probabilistic sampling methods.

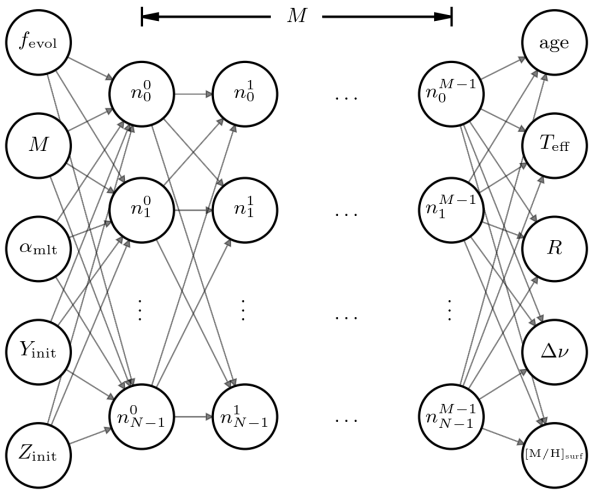

Figure 1. An artificial neural network comprising M hidden layers with N neurons per layer. Arrows connecting the nodes represent tunable weights.

We compared the performance of two optimisers: Adam (Kingma & Ba 2014) and stochastic gradient descent (SGD; see, e.g. Ruder 2016) with and without momentum (Qian 1999). Both optimizers required a choice of *learning rate* which determined the rate at which the weights were adjusted. We found that Adam performed well but the test loss was noisy as a function of epochs as it struggled to converge. The SGD optimizer was less noisy than Adam, but it was difficult to tune the learning rate. However, SGD with momentum allowed for more adaptive weight updates and outperformed the other configurations.

There are several ways to reduce over-fitting, from minimising the complexity of the architecture, to increasing the size and coverage of the training dataset. One alternative is to introduce weight regularisation. So-called L2 regularisation adds a term, $\sim \lambda_k \sum_i w_{i,k}^2$ to the loss function for a given hidden layer, k which acts to keep the weights small. We varied the magnitude of λ_k and found that if it was too large it would dominate the loss function, but if it was too small then performance on the test dataset was poorer.

We compared the choice of two error functions: mean squared error (MSE) and mean absolute error (MAE). The former is widely used amoung ANNs because it is more robust to outliers. However, we tracked both metrics regardless of which was added to the loss function and found that MAE converged faster. Although it is less robust to outliers, we were able to achieve sufficient accuracy faster with MAE.

After extensive tuning, we opted for an ANN with $N = 128$ neurons in each of $M = 6$ hidden layers. Each of the hidden layers used an ELU activation function and L2 weight regularisation with $\lambda = 1 \times 10^{-6}$. We trained the ANN for 50 000 epochs with a 500 training data batches each containing 15 472 input-ouptut pairs. To

fit the ANN, we used an SGD optimiser with an initial learning rate of 1×10^{-4} and momentum of 0.999 with an MAE loss function. Training took $\sim$ 48 h on an NVidia Tesla V100 graphics processing unit (GPU).

3.2.3 *Validation*

The validation dataset contains $\sim 2 \times 10^6$ models evolved in the same way as the training set but with randomly chosen initial conditions within the boundaries of the grid. We also constrained the validation dataset to $\tau < 15$ Gyr because ages above $\sim$ 15 yr are unphysical and such points are sparse in the training data. We made predictions for the validation dataset, deriving luminosity from the output radius and effective temperature, using the final trained ANN as described in Section 3.2.2. We then evaluated the accuracy of the ANN by taking the difference between the validation truth and prediction, $x_{\rm true} - x_{\rm pred}$.

We see from the summary statistics of the ANN error in Table 3 that the mean and median error lie sufficiently close to zero and the standard deviation is lower than, or of the order of typical model systematics discussed in the literature [CITE e.g. red giants challenge]. However, when we plot the error in Figure 2 we see that the standard deviation is a very conservative measure of the spread. The error distribution is Gaussian-like, but with large tails which arise from the use of the MAE loss function. Therefore, we also show the 68 and 95 per cent error intervals as a better indication of the ANN accuracy. The 68 per cent spread in $\Delta\nu$ error of $\sim \pm 0.1$ μHz is close to observational uncertainties for the highest signal-to-noise stars. [HOW DO I JUSTIFY THIS?] The accuracy of the other output observables are well below their respective observational uncertainties.

In Figure 2, we also show the distribution of each parameter in the validation dataset and a rolling error distribution as a function of each parameter. The accuracy of each parameter is best where there is the most training data, which is reflected in these plots.

To further justify the use of an ANN over interpolation, we timed a linear, multi-dimensional interpolator on small samples of size n from the training dataset. We used the Quickhall algorithm via the SCIPY package, for which the execution time scales by $n^{\lfloor d/2 \rfloor}$ for d dimensions (Barber et al. 1996). In our case $d = 5$, as such we found that interpolating the entire training dataset would take $\sim$ 2 yr using the same machine on which we trained the ANN. Furthermore, we interpolated a small region of the training dataset and evaluated its performance in the same region of the validation dataset. Taking the standard deviation of the error, we found that linear interpolation performed worse than the ANN by roughly a factor of 2.

3.3 Statistical models

We devised three Bayesian models, each with varying levels of parameter sharing between stars in the sample. Initially, we tested the models and demonstrated shrinkage of statistical uncertainties in the stellar fundamental parameters by analysing a random sample of 100 stars modelled using MESA. Then, we applied the models to the sample of stars collated in Section 2 and compared the results with that of S17.

The first model is equivalent to modelling each star individually and features no parameter sharing; as such, we refer to it as the no-pooled (NP) model. We then introduce two hierarchical Bayesian models (HBMs) which employ population-level parameters to describe their distribution in the sample. Both models partially-pool helium via a linear enrichment law. In other words, the initial helium fraction for each star is drawn from a normal distribution, with a mean described by the enrichment law and standard deviation to describe the deviation of helium from said law. One model also partially-pools the mixing-length theory parameter, $\alpha_{\rm mlt}$ in a similar way, whereas the other maximally-pools $\alpha_{\rm mlt}$ such that is assumes the same value for the entire sample. We refer to the former as the max-pooled (MP) model and the latter as the partial-pooled (PP) model. All three models are described in the following subsections.

We sampled the posterior for each model using the No U-Turn Sampler (NUTS) of PyMC4 [CITE]. Initially, we modelled each star individually in order to identify stars outside the grid range and other sampling problems. We flagged stars with median modelled values outside the grid range by more than the median 16th or 84th percentile in the sample.

3.3.1 *No-pooled model*

Firstly, we constructed a model comprising independent parameters $\boldsymbol{\theta}_i = \{f_{{\rm evol},i}, M_i, \alpha_{{\rm mlt},i}, Y_i, Z_i\}$ for a given star, i. Using Bayes' theorem, the *posterior* probability density function (PDF) of the model parameters given a set of observed data, $\boldsymbol{d}_i$ is,

$$p(\boldsymbol{\theta}_i|\boldsymbol{d}_i) \propto p(\boldsymbol{\theta}_i)\, p(\boldsymbol{d}_i|\boldsymbol{\theta}_i), \tag{8}$$

where $p(\boldsymbol{\theta}_i)$ is the *prior* PDF of the model parameters and $p(\boldsymbol{d}_i|\boldsymbol{\theta}_i)$ is the *likelihood* of observing the data given the model.

We chose weakly-informative, bounded priors for the independent parameters, restricting them to their respective ranges in the ANN training data. Although the neural network is able to make predictions outside the training data range, these have not been tested and may be unreliable. Therefore, we used a beta distribution with $\alpha = \beta = 1.2$ as the prior PDF on the independent parameters, transformed such that the probability is null outside the chosen range,

$$p(\boldsymbol{\theta}_i) = \prod_{k=1}^{N_\theta} \left[\theta_{k,\min} + (\theta_{k,\max} - \theta_{k,\min})\, \mathcal{B}(\theta_{k,i}|1.2, 1.2)\right], \tag{9}$$

where the beta distribution is defined as,

$$\mathcal{B}(x|\alpha,\beta) = \frac{x^{\,\alpha-1}(1-x)^{\beta-1}}{\int_0^1 u^{\,\alpha-1}(1-u)^{\beta-1}{\rm d}u}. \tag{10}$$

The beta distribution was preferred over a bounded uniform distribution because our sampler evaluates the gradient of the posterior and hence sensitive to discontinuities.

We made predictions for each star using the trained ANN, $\{\log(\tau)_i, T_{{\rm eff},i}, R_i, \Delta\nu_i, [{\rm M/H}]_{{\rm surf},i}\} = \boldsymbol{f}_{\rm ANN}(\boldsymbol{\theta}_i)$, from which we derived the luminosity, L_i using the Stefan-Boltzmann law. Any of the model parameters may be passed as an observable. Hereafter, we denote the set of model observables as $\boldsymbol{\mu}_{d,i} = \boldsymbol{f}(\boldsymbol{\theta}_i)$. Thus, we write the likelihood we observe any $\boldsymbol{d}_i$ with known uncertainty, $\boldsymbol{\sigma}_{d,i}$ given the model as,

$$p(\boldsymbol{d}_i|\boldsymbol{\theta}_i) = \prod_{k=1}^{N_{\rm obs}} \frac{1}{\sigma_{d,k,i}\sqrt{2\pi}} \exp\left[-\frac{(d_{k,i} - \mu_{d,k,i})^2}{2\sigma_{d,k,i}^2}\right], \tag{11}$$

where $N_{\rm obs}$ is the number of observed variables. We chose to use observed $T_{\rm eff}$, L, $\Delta\nu$ and [M/H] collated for our sample as described in Section 2.

Using the above model, we sampled from the posterior for each individual star separately and then together as a population of $N_{\rm stars}$

Table 3. Summary statistics of the absolute error between the validation dataset and the ANN predictions. The mean and standard deviation are represented by μ and σ and the percentiles denote the median, 68 and 95 per cent intervals.

Error	μ	σ	2.5%	16%	50%	84%	97.5%
$\tau^{\rm true} - \tau^{\rm pred}$ (Gyr)	0.0007	0.0132	-0.0223	-0.0082	-0.0001	0.0080	0.0339
$T_{\rm eff}^{\rm true} - T_{\rm eff}^{\rm pred}$ (K)	-0.2644	5.3958	-8.6254	-2.2231	-0.0999	1.4889	5.4073
$R^{\rm true} - R^{\rm pred}$ ($R_\odot$)	0.0003	0.0027	-0.0031	-0.0008	0.0000	0.0013	0.0057
$L^{\rm true} - L^{\rm pred}$ ($L_\odot$)	0.0027	0.0140	-0.0091	-0.0009	0.0008	0.0059	0.0271
$\Delta\nu^{\rm true} - \Delta\nu^{\rm pred}$ (μHz)	-0.0093	0.1853	-0.2757	-0.0980	-0.0071	0.0768	0.2254
$[{\rm M/H}]_{\rm surf}^{\rm true} - [{\rm M/H}]_{\rm surf}^{\rm pred}$ (dex)	-0.0000	0.0017	-0.0029	-0.0008	0.0000	0.0008	0.0026

stars,

$$p(\boldsymbol{\Theta}|\boldsymbol{D}) = \prod_{i=1}^{N_{\rm stars}} p(\boldsymbol{\theta}_i|\boldsymbol{d}_i). \tag{12}$$

Modelling stars separately allowed us to identify poorly sampled posteriors, whether the model indicated a fit outside the given input range, or other sampling issues. Once a refined sample was chosen, we modelled the sample all together as a natural application of the ANN through the use of batching. We modelled the ANN inputs as independent distributions, from which the random variables were batched together and passed through the ANN to produce predictions for each star. A graphical depiction of this model can be seen inside the grey box of Figure 3, without the arrow connecting $Z_{\rm init}$ to $Y_{\rm init}$.

3.3.2 *Partial-pooled model*

Sharing, or pooling parameters between stars in a population can improve the uncertainties on stellar fundamentals by encoding our prior knowledge of their distribution in a population. We constructed a hierarchical model [CITE Gelman?], which builds upon the NP model by introducing population-level *hyperparameters*. Specifically, we chose to describe initial helium and $\alpha_{\rm mlt}$ by partially-pooling them.

We constructed the PP model such that each of the initial helium, $\boldsymbol{Y}_{\rm init}$ and mixing-length theory parameter, $\boldsymbol{\alpha}_{\rm mlt}$ are drawn from a common distribution characterised by the set of hyperparameters, $\boldsymbol{\phi} = \{\Delta Y/\Delta Z, Y_P, \sigma_Y, \mu_\alpha, \sigma_\alpha\}$. Thus, Bayes' theorem becomes,

$$p(\boldsymbol{\phi}, \boldsymbol{\Theta}|\boldsymbol{D}) \propto p(\boldsymbol{\phi})\, p(\boldsymbol{Y}_{\rm init}, \boldsymbol{\alpha}_{\rm mlt}|\boldsymbol{\phi})\, p(\boldsymbol{f}_{\rm evol}, \boldsymbol{M}, \boldsymbol{Z})\, p(\boldsymbol{D}|\boldsymbol{\Theta}), \tag{13}$$

where $\boldsymbol{\Theta}$ is the same as in the NP model, i.e. each object-level parameter, $\boldsymbol{\theta}_j = \{\theta_{j,i}\}_{i=1}^{N_{\rm stars}}$.

We assumed the initial helium and the mixing-length parameter are each drawn from a normal distribution characterised by a population mean and standard deviation,

$$p(\boldsymbol{Y}_{\rm init}, \boldsymbol{\alpha}_{\rm mlt}|\boldsymbol{\phi}) = p(\boldsymbol{Y}_{\rm init}|\boldsymbol{\mu}_Y, \sigma_Y)\, p(\boldsymbol{\alpha}_{\rm mlt}|\mu_\alpha, \sigma_\alpha). \tag{14}$$

Regarding the first term of this equation, the mean initial helium follows a linear enrichment law with respect to the initial fraction of heavy-elements for a given star,

$$\boldsymbol{\mu}_Y = Y_P + \frac{\Delta Y}{\Delta Z}\boldsymbol{Z}_{\rm init}, \tag{15}$$

where Y_P is the primordial helium abundance fraction and $\Delta Y/\Delta Z$ is the so-called enrichment ratio. Therefore, we may write the prior PDF of initial helium given its population-level hyperparameters as,

$$p(\boldsymbol{Y}_{\rm init}|\boldsymbol{Z}_{\rm init}, \Delta Y/\Delta Z, Y_P, \sigma_Y) = \prod_{i=1}^{N_{\rm stars}} \mathcal{N}(Y_{{\rm init},i}|\mu_{Y,i}, \sigma_Y) \tag{16}$$

We justified this assumption based on theoretical and empirical evidence for a linear enrichment law [CITE], but taking into account an intrinsic spread, σ_Y about this law due to random variations in chemical abundance throughout the interstellar medium.

Similarly, for the second term of Equation 14, we chose to partially-pool the mixing-length parameter. We assume that convection in stars of a similar mass, evolutionary stage and area of the HR diagram may be approximated using a similar value of $\alpha_{\rm mlt}$, but the accuracy of the mixing-length theory may vary from star-to-star. There is theoretical evidence for such a variation with [M/H], $T_{\rm eff}$ and $\log g$ in 3D hydrodynamical stellar models (Magic et al. 2015; Viani et al. 2018). However, investigating such dependencies are beyond this scope of this paper. Given the small range of our sample, any such variation will be absorbed by the spread parameter, σ_α. Therefore, we decided to describe the prior on $\boldsymbol{\alpha}_{\rm mlt}$ as,

$$p(\boldsymbol{\alpha}_{\rm mlt}|\mu_\alpha, \sigma_\alpha) = \prod_{i=1}^{N_{\rm stars}} \mathcal{N}(\alpha_{{\rm mlt},i}|\mu_\alpha, \sigma_\alpha) \tag{17}$$

We gave all of the hyperparameters weakly informative priors, with the exception of Y_P for which we adopt a recent measurement of the primordial helium abundance the mean [CITE PLANK] with a standard deviation representative of the range of values in the literature [CITE]. We assumed priors on the hyperparameters as follows,

$$\begin{aligned}
\Delta Y/\Delta Z &\sim 4.0\,\mathcal{B}(1.2, 1.2),\\
Y_P &\sim \mathcal{N}(0.247, 0.1),\\
\sigma_Y &\sim \mathcal{LN}(0.01, 1.0),\\
\mu_\alpha &\sim 1.5 + \mathcal{B}(1.2, 1.2),\\
\sigma_\alpha &\sim \mathcal{LN}(0.1, 1.0),
\end{aligned}$$

where, for instance, $x \sim \mathcal{LN}(m, \sigma)$ represents a random variable drawn from the log-normal distribution,

$$\mathcal{LN}(x|m, \sigma) = \frac{1}{x\sigma\sqrt{2\pi}} \exp\left[-\frac{\ln(x/m)^2}{2\sigma^2}\right]. \tag{18}$$

3.3.3 *Max-pooled model*

We built another hierarchical model similar to the PP model except that $\alpha_{\rm mlt}$ is max-pooled. In other words, we assumed that the mixing length must be the same value for every star in the sample, but still allowed it to freely vary. Thus the hyperparameters are now, $\boldsymbol{\phi} = \{\Delta Y/\Delta Z, Y_P, \sigma_Y, \alpha_{\rm mlt}\}$. The posterior distribution of the model takes the same form as in Equation 13 except that now,

$$p(\boldsymbol{\alpha}_{\rm mlt}|\alpha_{\rm mlt}) = \prod_{i=1}^{N_{\rm stars}} \delta(\alpha_{{\rm mlt},i}|\alpha_{\rm mlt}) \tag{19}$$

where $\delta(x|\alpha)$ is defined as,

$$\delta(x|\alpha) = \begin{cases} +\infty, & x = \alpha \\ 0, & x \neq \alpha \end{cases} \quad (20)$$

4 RESULTS

We obtained model stellar fundamental parameters for the set of test stars and the sample obtained in Section 2. For each of the NP, PP and MP models, we took the median and 68 percent credible region from the marginalised posterior samples. In this section, we present the results from the test dataset and compare them to the tue values. We then present the results for the *Kepler* dwarfs and compare the results to S17.

4.1 Test stars

We found good agreement with the true values in the test sample. In Figure 4 we show the z-score, for the population of a given parameter, x,

$$z = \frac{\bar{x} - x_{true}}{s_x}, \quad (21)$$

where $\bar{x}$ and s_x are the sample mean and standard deviation in x from the modelled posterior. We see that the NP model underestimates the residules because its z-score is narrower than an $\mathcal{N}(0, 1)$ distribution. We expected this is due to the poorly constrained parameters, $\alpha_{\rm mlt}$ and $Y_{\rm init}$, for which their marginalised posteriors were not Gaussian (see Figure **??**). Boundary effects for these parameters bias their mean values towards the centre of the prior which reduces the difference between the truth and sample mean relative to the uncertainty in said parameter. We see this effect reduce in the PP and MP models because pooling the parameters together improves parameter uncertainties, reducing sampling at the prior boundaries.

We also found that all the models produced systematically low ages and high masses. Pooling the parameters reduced the parameter uncertainty which further exaggerated these differences. We show the z-score for the test observables compared to their true values in Figure 5. We notice that the observed $\Delta\nu$ was systematically high and L systematically low. The combination of these effects are likely the cause of the systematic shift in model results, because they are consistent across all the models. Therefore, we note that reducing the statistical uncertainties on stellar fundamental parameters will help highlight the effects of systematic uncertainties in the observed parameters.

We confirmed that the uncertainties on mass, age and radius decrease with increasing sample size in the PP model.

Fitting the helium enrichment law and spread in mixing-length to the NP model results recovered the true hyperparameters with higher precision than the PP and MP models. However, fitting this way limited the precision of the stellar parameters, wheras the hierarchical models reduced the uncertainties by roughly a factor of $\sqrt{N_{\rm stars}}$. The results for the test stars are shown in more detail in Appendix **??**.

4.2 Real stars

With confidence that the models were able to obtain accurate stellar parameters, in accordance with our choice of stellar models, we present results for the sample of 81 *Kepler* dwarfs for each of our statistical models. Tables of results for each model are available for download at TODO.

We obtained results for the hyperparameters in each of the models and present them in Table 4. For NP, we fit the same hyperparameters from the PP model to the results from the NP model, using the same prior distributions.

The PP and MP results without the Sun are self-consistent, but the biggest difference between the two methods is evident when the Sun is added. The MP model will typically settle for a shared value of $\alpha_{\rm mlt}$ which favours the star with the best observational constraints. In our case, the solar model yields $\alpha_{\rm mlt} = 2.11^{+0.01}_{-0.01}$ which is far from $\alpha_{\rm mlt}$ of $1.73^{+0.08}_{-0.07}$ obtained without the Sun. However, when $\alpha_{\rm mlt}$ is partially-pooled, the σ_α parameter copes with this by increasing to include the Sun in the distribution. The PP models are more robust.

We noticed that the uncertainties on the NP hyperparameters were smaller than those of the hierarchical models. However, these are likely underestimated because the NP model poorly constrains $\alpha_{\rm mlt}$ and $Y_{\rm init}$ such that the bounds of the prior have the effect of reducing the standard deviation of their marginalized posteriors. On the contrary, the hierarchical models SOMETHING. . .

We found that including the sun in our PP and MP models systematically shifted the median ages of the sample by about 0.5 Gyr and 1.0 Gyr respectively (Figure **??**). This is a direct result of the solar model favouring a higher $\alpha_{\rm mlt}$ and lower $Y_{\rm init}$ than the rest of the sample. Partially pooling the sun with the rest of the sample copes with this better by accounting for a population spread in the parameters, hence the smaller difference with and without the Sun.

5 DISCUSSION

We have shown that, utilising hierarchical models, it is possible to reduce the statistical uncertainties on fundamental stellar parameters by sharing information between the stars. However, as such uncertainties reduce, systematics begin to dominate. We stress that the next challenge is to robustly model the systematic uncertainties between stellar modelling codes and within observables. Until then, we hesitate to publish one preferred set of parameters for our sample of stars. Instead, this paper is a demonstration of our method.

6 CONCLUSIONS

ACKNOWLEDGEMENTS

REFERENCES

Asplund M., Grevesse N., Sauval A. J., Scott P., 2009, ARA&A, 47, 481
Barber C. B., Dobkin D. P., Huhdanpaa H., 1996, ACM Trans. Math. Softw., 22, 469
Clevert D.-A., Unterthiner T., Hochreiter S., 2015, arXiv e-prints, 1511, arXiv:1511.07289
Ferguson J. W., Alexander D. R., Allard F., Barman T., Bodnarik J. G., Hauschildt P. H., Heffner-Wong A., Tamanai A., 2005, The Astrophysical Journal, 623, 585
Glorot X., Bordes A., Bengio Y., 2011, Proc. 14th Int. Conf. Artif. Intell. Statisitics AISTATS 2011, 15, 315
Hahnloser R. H. R., Sarpeshkar R., Mahowald M. A., Douglas R. J., Seung H. S., 2000, Nature, 405, 947
Huber D., et al., 2011, ApJ, 743, 143
Kingma D. P., Ba J., 2014, arXiv e-prints, 1412, arXiv:1412.6980
Magic Z., Weiss A., Asplund M., 2015, A&A, 573, A89
Paxton B., Bildsten L., Dotter A., Herwig F., Lesaffre P., Timmes F., 2011, ApJS, 192, 3

Table 4. Hyperparameter results for each model in descending order of the helium enrichment ratio, $\Delta Y/\Delta Z$.

Model	$\Delta Y/\Delta Z$	Y_P	σ_Y	μ_α	σ_α	$\alpha_{\rm mlt}$
NP	$1.69^{+0.21}_{-0.21}$	$0.247^{+0.001}_{-0.001}$	$0.0074^{+0.0026}_{-0.0022}$	$1.95^{+0.04}_{-0.04}$	$0.06^{+0.03}_{-0.02}$	—
MP	$1.60^{+0.45}_{-0.42}$	$0.247^{+0.001}_{-0.001}$	$0.0051^{+0.0044}_{-0.0027}$	—	—	$1.73^{+0.08}_{-0.07}$
PP	$1.60^{+0.45}_{-0.42}$	$0.247^{+0.001}_{-0.001}$	$0.0051^{+0.0045}_{-0.0027}$	$1.74^{+0.08}_{-0.07}$	$0.06^{+0.05}_{-0.03}$	—
PPS	$1.05^{+0.28}_{-0.25}$	$0.247^{+0.001}_{-0.001}$	$0.0045^{+0.0038}_{-0.0023}$	$1.90^{+0.09}_{-0.09}$	$0.13^{+0.06}_{-0.05}$	—
MPS	$0.76^{+0.24}_{-0.27}$	$0.247^{+0.001}_{-0.001}$	$0.0049^{+0.0039}_{-0.0025}$	—	—	$2.09^{+0.03}_{-0.03}$

Paxton B., et al., 2013, The Astrophysical Journal Supplement Series, 208, 4
Paxton B., et al., 2015, The Astrophysical Journal Supplement Series, 220, 15
Paxton B., et al., 2018, The Astrophysical Journal Supplement Series, 234, 34
Paxton B., et al., 2019, The Astrophysical Journal Supplement Series, 243, 10
Qian N., 1999, Neural Networks, 12, 145
Rogers F. J., Nayfonov A., 2002, The Astrophysical Journal, 576, 1064
Ruder S., 2016, arXiv e-prints, 1609, arXiv:1609.04747
Serenelli A., et al., 2017, ApJS, 233, 23
Townsend R. H. D., Teitler S. A., 2013, Monthly Notices of the Royal Astronomical Society, 435, 3406
Viani L. S., Basu S., Ong J. M. J., Bonaca A., Chaplin W. J., 2018, The Astrophysical Journal, 858, 28
White T. R., Bedding T. R., Stello D., Christensen-Dalsgaard J., Huber D., Kjeldsen H., 2011, The Astrophysical Journal, 743, 161
Zinn J. C., Pinsonneault M. H., Huber D., Stello D., Stassun K., Serenelli A., 2019, ApJ, 885, 166

APPENDIX A: NEURAL NETWORK

APPENDIX B: TESTING THE METHOD

We tested the ability of the method to recover stellar fundamental properties in accordance with our choice of stellar evolution code and physics.

This paper has been typeset from a TEX/LATEX file prepared by the author.

Table A1. The median, $\mu_{1/2}$ and standard deviation, σ for each parameter in the training data, used to standardise the dataset.

	Input					**Output**				
	$f_{\rm evol}$	M ($M_\odot$)	$\alpha_{\rm mlt}$	$Y_{\rm init}$	$Z_{\rm init}$	log(age/Gyr)	$T_{\rm eff}$ (K)	R ($R_\odot$)	$\Delta\nu$ (μHz)	$[M/H]_{\rm surf}$ (dex)
$\mu_{1/2}$	0.865	1.000	1.900	0.280	0.017	0.790	5566.772	1.224	100.720	0.081
σ	0.651	0.118	0.338	0.028	0.011	0.467	601.172	0.503	42.582	0.361

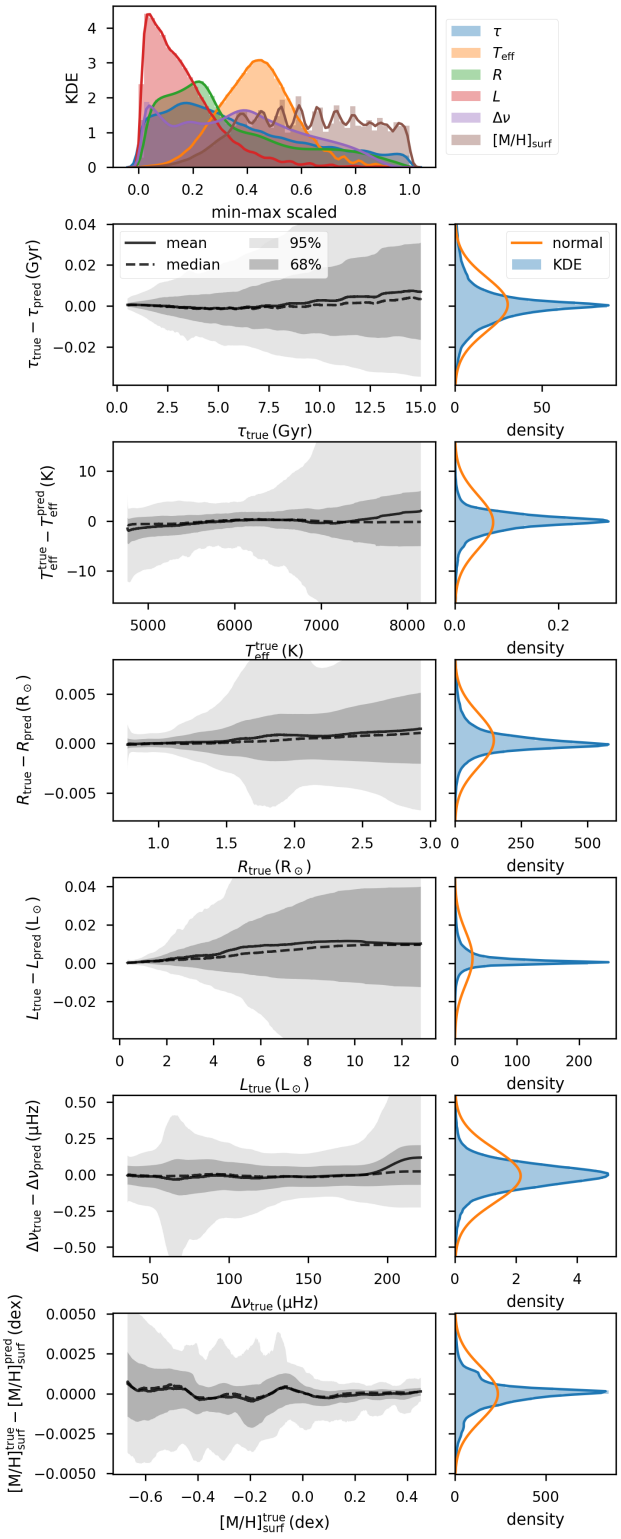

Figure 2.

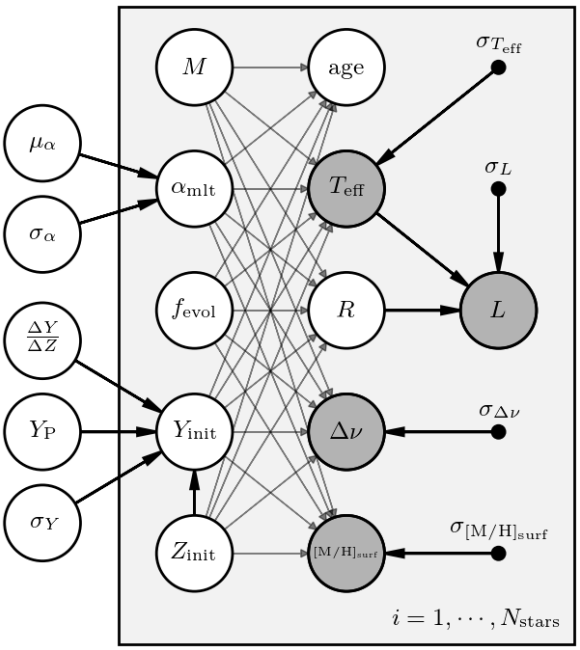

Figure 3.

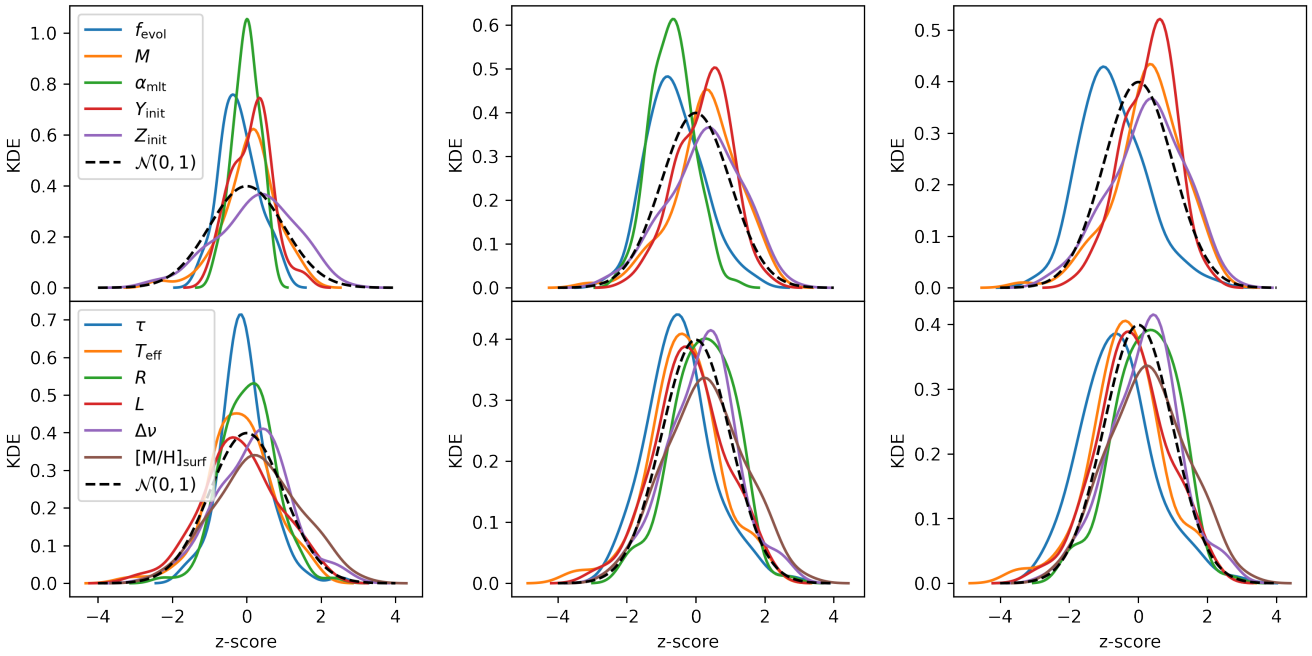

(a) NP (b) PP (c) MP

Figure 4.

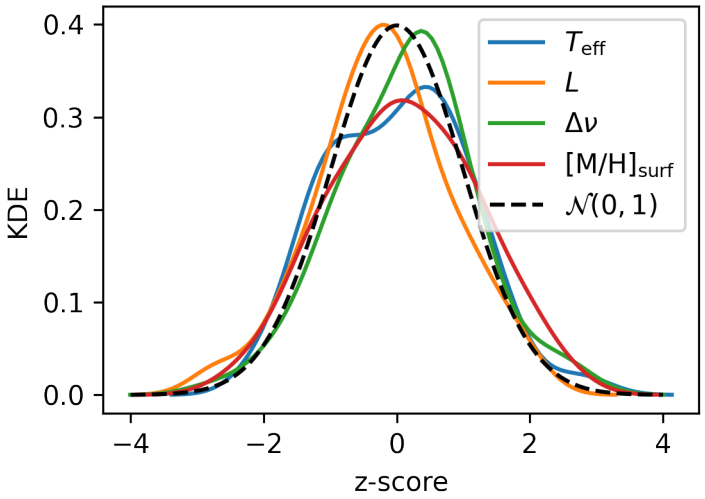

Figure 5.

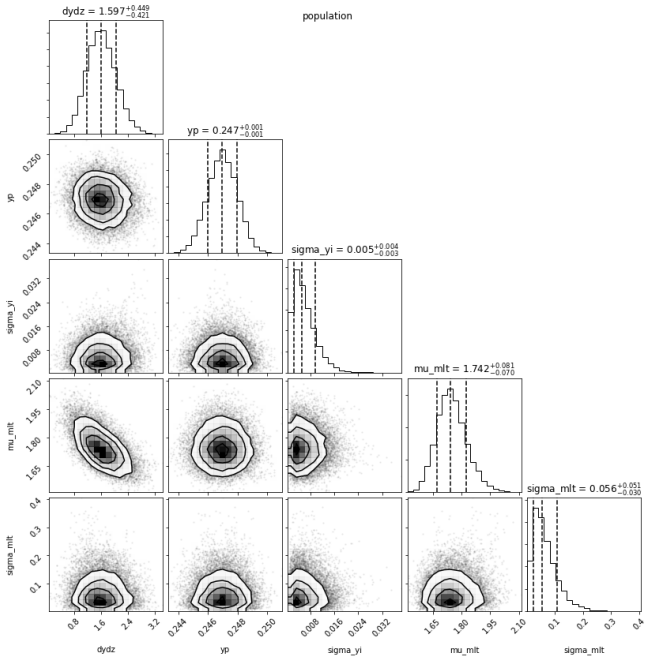

(a) Population hyperparameters for model without the Sun.

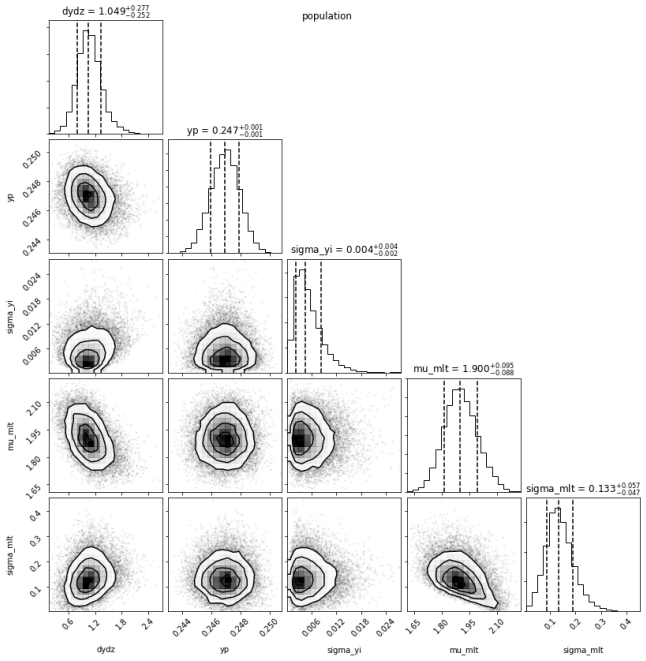

(b) Population hyperparameters for model with the Sun.

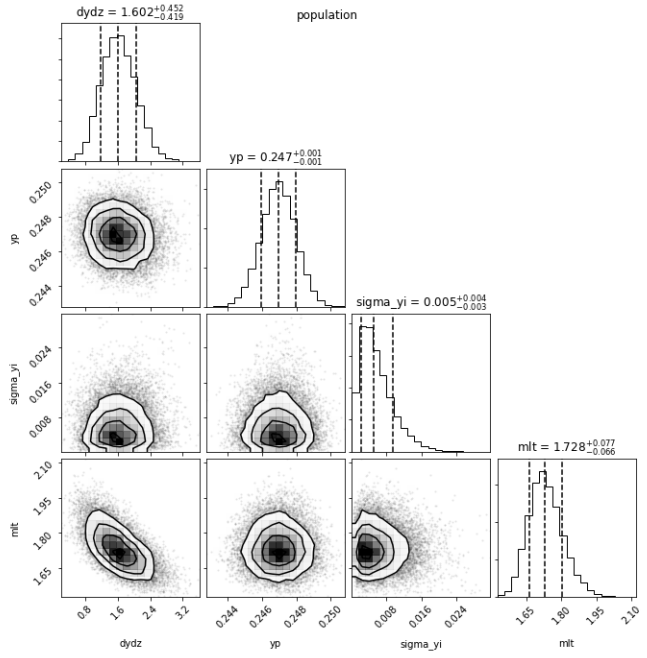

(c) Population hyperparameters for model without the Sun.

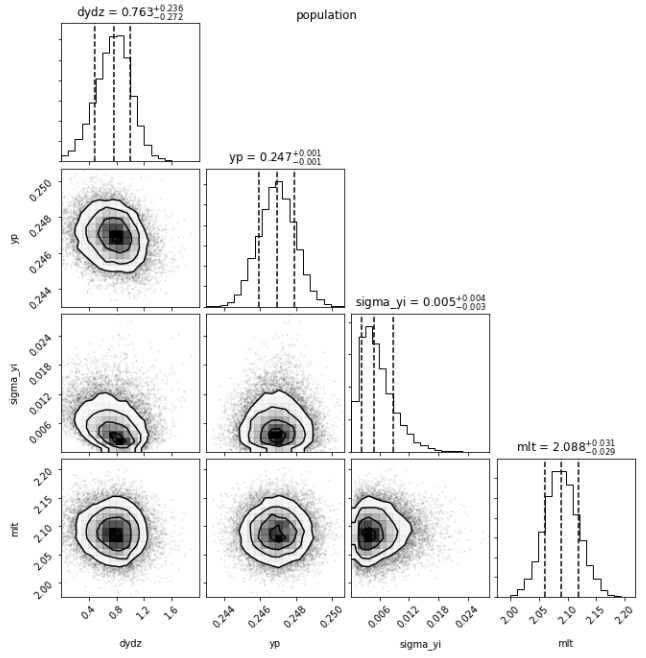

(d) Population hyperparameters for model with the Sun.

Figure 6.

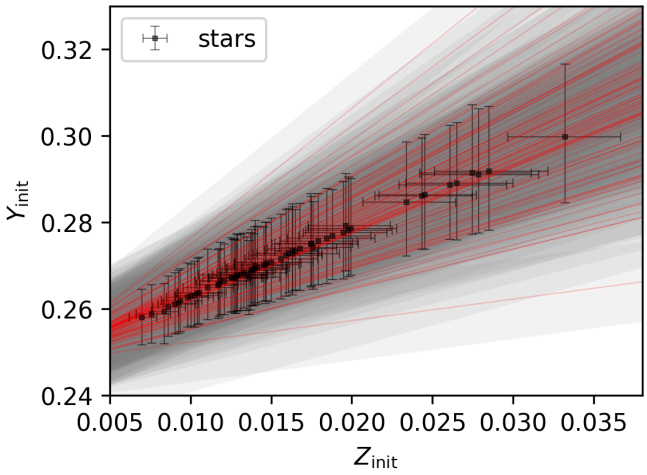

(a)

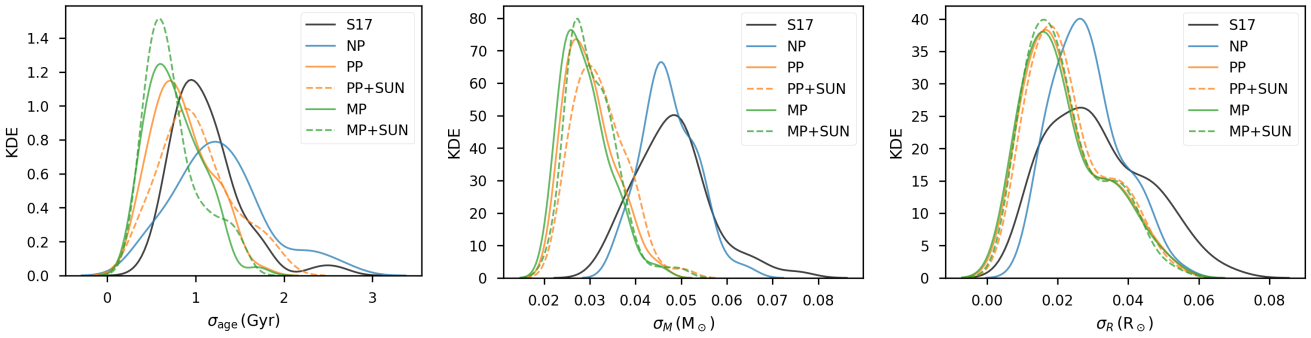

(a) Age (b) Mass (c) Radius

Figure 8. Kernel density estimates (KDEs) of the uncertainties in the results from each model compared with that of (S17).